[Papers in Palaeontology, Vol. 11, Part 6, 2025, e70045]

Systematic utility of the phytosaur post-dentary mandibular region

by VÍCTOR LÓPEZ-ROJAS[1,2,*], MIGUEL MORENO-AZANZA[1,2,3] *and* EDUARDO PUÉRTOLAS-PASCUAL[1,2,3]

[1]GeoBioTec, Faculdade de Ciências e Tecnologia da Universidade Nova de Lisboa, 2829–516 Monte de Caparica, Portugal; v.rojas@campus.fct.unl.pt, mmazanza@unizar.es, puertolas@unizar.es
[2]Museu da Lourinhã, Rua João Luís de Moura 95, 2530–158 Lourinhã, Portugal
[3]Aragosaurus–IUCA Recursos Geológicos y Paleoambientes, Universidad de Zaragoza, C/ Pedro Cerbuna 12, 50009 Zaragoza, Spain
*Corresponding author

Typescript received 5 December 2024; accepted in revised form 19 September 2025

Abstract: Phytosaurs, crocodile-like archosaurs from the Late Triassic, are known for their unique skull shape, whereas their mandibles are poorly studied. Two-dimensional (2D) geometric morphometric (GM) analysis is commonly used on dinosaurs and mammals. We applied this technique for the first time to the study of phytosaur mandibles to identify and quantify morphological differences outside the skull for use in phylogenetic analysis. The 2D GM analysis showed that the dorsal shape of the surangular had significant phylogenetic utility. This led to the reformulation of two characters (shape of the dorsal margin of the surangular, and shape of the retroarticular process) and the creation of four more new characters: shape of the ventral margin of the angular, dorsoventral height of the external mandibular fenestra, suture between the dentary and surangular, and the dorsal margin transition angle between the dentary and the surangular. Furthermore, three of these were identified as synapomorphies for the clade Leptosuchomorpha. To test the hypothesis that the mandible is taxonomically relevant, we ran a second analysis including two problematic, mandible specimens: NOVA-FCT-DCT 5396 (Silves Group, Portugal); and NMMNHS P-4256 (Bull Canyon Formation, New Mexico; which has been referred to *Machaeroprosopus* and *Redondasaurus* in previous studies). The analysis provided better resolution for these indeterminate specimens, suggesting that NOVA-FCT-DCT 5396 is *Angistorhinus* cf. *talainti*, and NMMNHS P-4256 is cf. *Machaeroprosopus* (Mystriosuchini).

Key words: post-dentary, Phytosauria, Triassic, phylogeny, geometric morphometrics.

PHYTOSAURS are well-known crocodile-like archosaurs from the Late Triassic worldwide (Chatterjee 1978; Stocker & Butler 2013; Jones & Butler 2018; López-Rojas *et al.* 2022; Datta & Ray 2023). Phytosaur taxonomical research has focused on the skull (e.g. Ballew 1989; Nesbitt 2011; Jones & Butler 2018; Datta *et al.* 2021), with special discussion on the squamosal morphology for taxonomic discrimination within leptosuchomorphs (Parker & Irmis 2006), although mandibles, axial and appendicular remains have also been collected (Case 1922, 1927, 1932; Long & Murry 1995; Hunt *et al.* 2002; Zeigler *et al.* 2003; Mateus *et al.* 2014; Griffin *et al.* 2017; Butler *et al.* 2019; Heckert *et al.* 2021), as well as almost complete skeletons (Gozzi & Renesto 2003; Stocker *et al.* 2017).

The posterodorsal migration of the external nares and the strong modification of the skull are characteristic of this clade. Almost two-thirds of the skull length is composed of an elongated rostrum, primarily the tooth-bearing bones (premaxilla and maxilla), whereas the non-tooth-bearing bones were relegated to a reduced posterior portion of the skull. A similar modification is found in the mandible, two-thirds of which is composed of a long dentary. These modifications resulted in highly variable morphology in the post-dentary bones, which run parallel to the posterior region of the skull, with potential taxonomic value that has hitherto received little attention. Despite the existence of copious, rich and diverse remains, most of the focus has been on the upper portion of the skull. Only general phylogenetic studies regarding archosauromorphs have used axial and appendicular material of phytosaurs (Nesbitt 2011; Ezcurra 2016), whereas mandibular and postcranial material have been neglected in phylogenetic works at the genus level. The most recent extensive phylogenetic study of phytosaurs was by Jones & Butler (2018), with 94 characters. Of these, only three were lower jaw characters (length of the mandibular symphysis, shape of the dorsal region of the surangular, and shape of the retroarticular process), and there were no axial or

doi: 10.1002/spp2.70045

appendicular characters. Two new Late Triassic species, *Mystriosuchus alleroq* López-Rojas *et al.* 2022 from the middle Norian of East Greenland, and *Colossosuchus techniensis* Datta & Ray 2023 from the upper Carnian to lower–middle Norian of India, shed light on the phytosaur jaw and non-skull regions. Even though one dental character was added in López-Rojas *et al.* (2022; char. 95) (Fig. 1A) based on Hungerbühler (2000), these authors provided an extensive description and comparison of the postcranial remains of phytosaurs. In contrast, Datta & Ray (2023) (Fig. 1B) added a total of 11 new characters, nine of which were non-skull focused (axial and appendicular characters).

Studies of these 'less informative' bones have mostly been restricted to palaeoecological analyses. For example, some early research attempted to illustrate the lifestyles of these animals based on these body regions (Anderson 1938; Long & Murry 1995; Zeigler *et al.* 2003). More recent studies have focused on their terrestrial or aquatic affinities (Kimmig 2013; Butler *et al.* 2019), their ontogeny (Heckert *et al.* 2013), and the presence of convergent structures and lifestyle similarities with crocodylians (Lemanis *et al.* 2019; Bona *et al.* 2022) and also spinosauroids (Yun 2024).

Outside Phytosauria, the mandibular region posterior to the dentary is well documented and has been the object of a variety of studies, focusing for example on: the evolution and homology of the mandible among archosauriforms (Bona *et al.* 2022); or muscle attachments and bite forces (Anderson 1938; Holloway 2018; Holliday 2019; Holliday *et al.* 2022). These previous studies enable comparison between extinct and extant pseudosuchians (Sellers *et al.* 2022), and even with the flat-shaped skulls of older archosauriforms such as proterochampsids (De Simão-Oliveira *et al.* 2024). Despite the strong modification of phytosaur mandibles, their potential taxonomical importance has been neglected. Only a few studies have investigated the new potential taxonomic information of the mandibular (Hungerbühler 2000; Heckert *et al.* 2013) and postcranial regions of phytosaurs (Griffin *et al.* 2017; Goldsmith *et al.* 2024; LePore & McLain 2024).

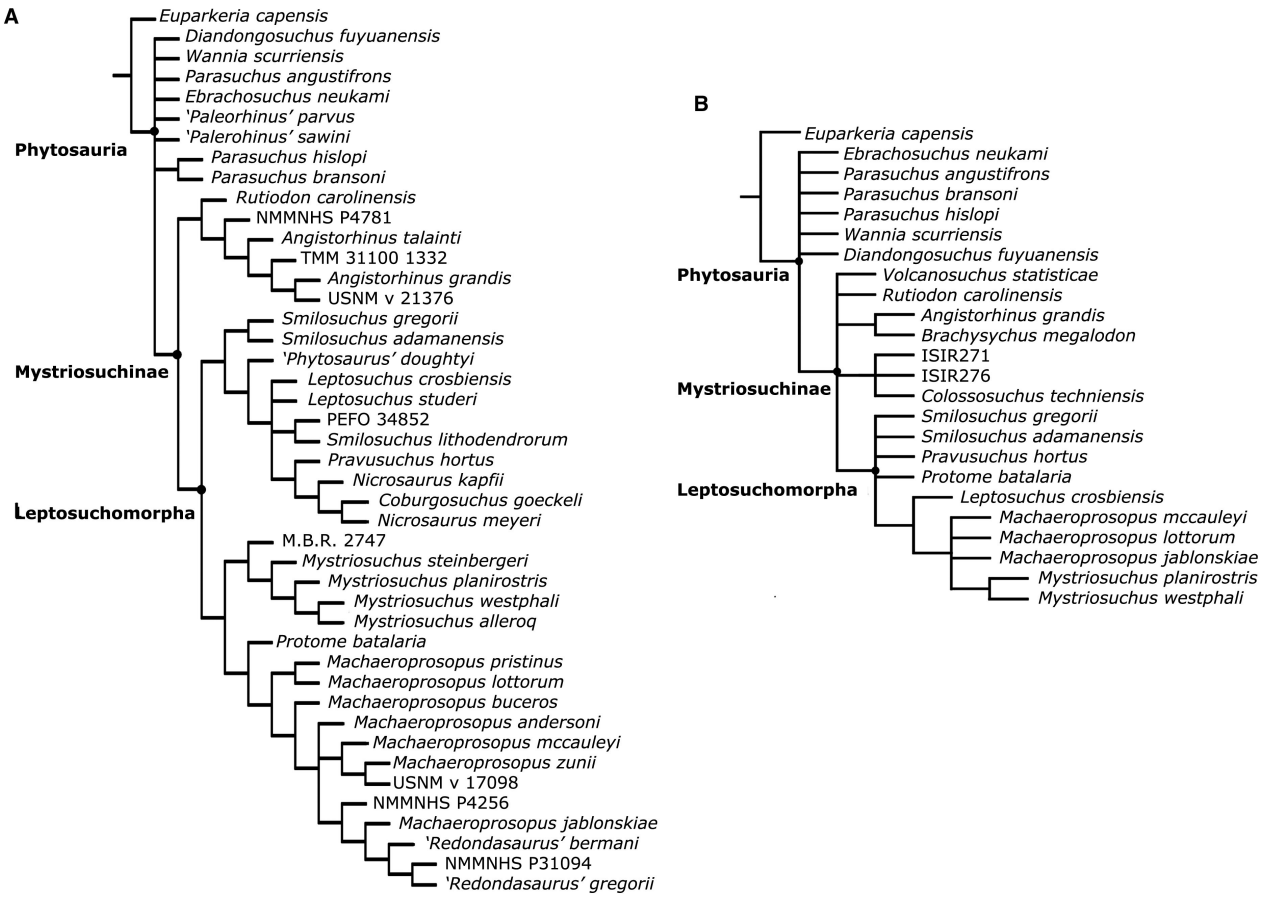

FIG. 1. A, strict consensus tree from López-Rojas *et al.* (2022), with the addition of the species *Mystriosuchus alleroq*, from Greenland. B, strict consensus tree from Datta & Ray (2023), with the addition of the species *Colossosuchus techniensis*, from India.

GEOMETRIC MORPHOMETRICS AS A SOURCE OF NEW CHARACTERS FOR PHYLOGENETIC ANALYSIS

The use of two-dimensional (2D) geometric morphometric analyses based on landmarks and semi-landmarks has previously featured in the studies of a variety of groups, including insects (Changbunjong *et al.* 2023), mammals (McGuire 2011; Jansky *et al.* 2016), and dinosaurs (Maiorino *et al.* 2013; Prieto-Márquez *et al.* 2020; Kobayashi *et al.* 2022). The technique has been used to discern taxon differentiation in some of these groups, with better results in mammals (Jansky *et al.* 2016, with over 80% confidence) than in dinosaurs (Prieto-Márquez *et al.* 2020). Holvast *et al.* (2024) conducted an exhaustive search to determine to what extent the phylogenetic analyses are improved by the incorporation of morphometric data (landmark-based and continuous) compared with only discrete character-based analysis. Although morphometric data have proven valuable in research on macroevolution (Bona *et al.* 2022; Allemand *et al.* 2023) and in understanding the functional biology and development of structures (Pereira-Pedro *et al.* 2020; Allemand *et al.* 2023), Holvast *et al.* (2024) found no improvement in phylogenetic analysis when using morphometric data, alone or combined with discrete characters, under current models.

The use of landmark-based morphometric analyses in studies of phytosaurs is limited, being restricted, like most research on phytosaurs, to the skull (Jones & Butler 2018; Datta *et al.* 2021). This technique has been used to improve the resolution of poorly supported nodes (*Machaeroprosopus* taxa in Jones & Butler 2018) or for lifestyle and cranial evolution (Datta *et al.* 2021).

Here, we focus on the post-dentary bones (surangular, articular, retroarticular, angular, splenial) and the external mandibular fenestra of the phytosaur mandible, and apply 2D geometric morphometric landmark- and semi-landmark-based analysis to study this region of the mandible. These analyses make it possible to describe new morphological features shared between clades, which are then used in phylogenetic analyses. The new data provided by these analyses will help to resolve the intricate taxonomic relationships among phytosaurs, as well as provide additional characters that aid in classifying isolated mandible material from phytosaurs.

MATERIAL & METHOD

Material

Landmark data were acquired from photographs of specimens examined in person and from the original published figures of specimens that could not be examined directly, resulting in a total of 20 landmarked specimens. Of these, 14 species of phytosaurs were represented in the sample (Table 1), most of which were used in previous phylogenetic studies (Nesbitt 2011; Jones & Butler 2018; Datta & Ray 2023).

In addition, another two specimens were introduced into the analysis to test our hypothesis on the phylogenetic significance of the mandible. These are: the indeterminate specimen mandible NOVA-FCT-DCT 5396 (published in Mateus *et al.* 2014 as FCT-UNL 700, its catalogue number having recently been changed due to an update of collections) from the Silves Group, Penina locality, Portugal, and hosted in the Museu de Loulé in Portugal; and the specimen NMMNHS P-4256, from the Bull Canyon Formation, New Mexico, and hosted in the New Mexico Museum of Natural History and Science, Albuquerque, NM, USA.

The partial right mandible of the indeterminate phytosaur NOVA-FCT-DCT 5396 (Mateus *et al.* 2014) was discovered geographically and stratigraphically close to the *Metoposaurus* bone bed at Penina locality (Algarve Basin, South Portugal). It was found in the Marl-Carbonate Evaporitic Complex of the Silves Group, which crops out north of the Algibre Fault (Vilas-Boas *et al.* 2024), sometimes referred to as the Grés de Silves Formation (e.g. Mateus *et al.* 2014). Initially, the Algarve Basin was thought to date back to the Early Jurassic due to the presence of Tethyan ammonites (Nomade *et al.* 2007; Verati *et al.* 2007) associated with Triassic rifting (Terrinha *et al.* 2002). However, recent palynological research by Vilas-Boas *et al.* (2024) has revised the age of the Silves Group, updating this section to the late Carnian age. This finding aligns with previous indications of late Carnian or early Norian age suggested by Brusatte *et al.* (2015), based on the presence of a *Metoposaurus*-dominated temnospondyl fauna. Additionally, this timeframe corresponds more closely to that of North Morocco, which has a similar and related amphibian temnospondyl fauna. Although there are other archosauromorph remains that possibly relate to phytosaurs in eastern Spain (Ezcurra *et al.* 2017; Berrocal-Casero *et al.* 2018), the indeterminate phytosaur from south Portugal is the only indisputable phytosaur of the Iberian Peninsula.

Furthermore, the Iberian phytosaur NOVA-FCT-DCT 5396 has a process dorsally projected from the angular that Mateus *et al.* (2014) described as a 'coronoid process', in medial view. However, as explained by Bona *et al.* (2022), phytosaurs, like other pseudosuchian taxa such as aetosaurs and notosuchian crocodylomorphs, lack this medial coronoid process. Therefore, this 'coronoid process' is likely to be either the posterior-most region of the splenial, as preserved in *Mystriosuchus alleroq* (López-Rojas *et al.* 2022), or a projection of the prearticular, as described in Bona *et al.* (2022) for the mandible of *Nicrosaurus kapffi*.

TABLE 1. Phytosaur mandible specimens and corresponding information.

Genus	Species	Collection no.	Type of material	First description	References
Angistorhinus	*talainti*	MNHN F-TAL 3	Holotype	Dutuit (1977a)	Dutuit (1977b)
Angistorhinus	*talainti*	MNHN F-TAL 4	Referred material for comparison	Dutuit (1977a)	Dutuit (1977b)
Angistorhinus	*talainti*	MNHN F-TAL 7	Referred material for comparison	Dutuit (1977a)	Dutuit (1977b)
Diandongosuchus	*fuyuanensis*	ZMNH M8770	Holotype	Li *et al.* (2012)	Stocker *et al.* (2017) (*sensu*)
Machaeroprosopus	*buceros*	NMMNHS P-36051	Referred material	Cope (1881)	Jones & Butler (2018)
Machaeroprosopus	*mccauleyi*	UCMP 126999	Specimen previously used for scoring	Ballew (1989)	Jones & Butler (2018)
Machaeroprosopus	*pristinus*	UCMP 27018	Specimen previously used for scoring	Mehl (1928)	Jones & Butler (2018)
Machaeroprosopus	*pristinus*	UCMP 7043/27018	Specimen previously used for scoring	Mehl (1928)	Jones & Butler (2018)
Nicrosaurus	*kapffi*	SMNS 5730	Referred material	Meyer (1860)	Jones & Butler (2018)
Mystriosuchus	*alleroq*	NHMD 916731	Holotype	López-Rojas *et al.* (2022)	López-Rojas *et al.* (2022)
Mystriosuchus	*planirostris*	SMNS 10260	Specimen previously used for scoring	Meyer (1863)	Jones & Butler (2018)
Mystriosuchus	*planirostris*	SMNS 9900	Specimen previously used for scoring	Meyer (1863)	Jones & Butler (2018)
Mystriosuchus	*planirostris*	SMNS 91574	Specimen previously used for scoring	Meyer (1863)	Jones & Butler (2018)
'*Paleorhinus*'	cf. *arenaceus*	ZPAL An III 3592	Provisional name, phylogenetic analysis in work by Polish team	Fraas (1896)	Dzik & Sulej (2007)
Parasuchus	*hislopi*	ISI R42	Neotype	Lydekker (1885)	Kammerer *et al.* (2016) (neotype)
Protome	*batalaria*	PEFO 34034	Holotype	Stocker (2012)	Stocker (2012)
Smilosuchus	*adamanensis*	UCMP 26699	Holotype	Camp (1930)	Camp (1930)
Smilosuchus	*gregorii*	UCMP A272/27200	Holotype	Camp (1930)	Camp (1930)
Redondasaurus	*bermani*	CMNH 69727	Holotype	Hunt & Lucas (1993)	Rinehart *et al.* (2009)
Euparkeria	*capensis*	SAM-PK-5867	Holotype	Broom (1913)	Jones & Butler (2018)
Phytosauria indet.	–	NOVA-FCT-DCT 5396	Partial mandible	Mateus *et al.* (2014)	Mateus *et al.* (2014)
Machaeroprosopus?	–	NMMNHS P-4256	Specimen previously used for scoring	Hunt (1994)	Jones & Butler (2018)

Specimen NMMNHS P-4256 has previously been the object of a study on sexual dimorphism in phytosaurs by Hunt *et al.* (2006), in which it was assigned to '*Pseudopalatus*' *mccauleyi*. Given that the taxon '*Pseudopalatus*' has since been synonymized with *Machaeroprosopus* (Parker *et al.* 2013), specimen NMMNHS P-4256 was subsequently renamed *Machaeroprosopus mccauleyi*. However, this specimen has also been tentatively referred to *Redondasaurus* (Hunt 1994; Heckert *et al.* 2001); Jones & Butler (2018) attempted to resolve the genus using a phylogenetic analysis with discrete, continuous and landmark characters. They concluded that NMMNHS P-4256 was potentially *Machaeroprosopus*, sharing its features and biozone with *Ma. jablonskiae* and *Ma. mccauleyi*. Our aim was to test its placement using a different analysis, focusing on the lower jaw material, with a view to clarifying the previous results. Several limitations arose from the scarcity of available material and the lack of accessible information. In the case of *Mystriosuchus steinbergeri* Butler *et al.* 2019, the mandible remains (NHMW

1986/0024/0002) in lateral view are poorly preserved, missing half of the posterior region in the left mandible, and also missing the dorsal region in the right mandible (Butler *et al.* 2019, fig. 10). In the case of other phytosaurs, such as *Wannia scurrensis* Langston 1949 (TTU P-00539) (*sensu* Stocker 2013), *Ebrachosuchus neukami* Kuhn 1936 (BSPG 1931 X 501), '*Paleorhinus*' *magnoculus* Dutuit 1977a (MNHN ALM 1), '*Paleorhinus*' *angustifrons* Kuhn 1936 (BSPG 1931 X 502) (*sensu* Butler *et al.* 2014), and *Mystriosuchus westphali* Hungerbühler 2002 (GPIT 261/001), no related mandible remains are described or available. In addition, Fara & Hungerbühler (2000) indicated that the specimen of '*Paleorhinus*' *magnoculus* potentially belongs to a juvenile, also making it unfit for our analysis. Some of the partial mandibles not included in the geometric morphometrics analysis were instead used for morphological comparison afterwards based on phylogenetic relationships.

The phytosaur species *Angistorhinus talainti* Dutuit 1977b presented challenges for morphometric analyses. The holotype mandible (MNHN F-TAL 3) is mostly complete, but it is missing the retroarticular process. Additionally, the posterior region of the dentary (both dorsal and ventral) is distorted and not straight. This presented a problem for accurate placement of landmarks on different regions of the mandible. However, we used the partial mandibles MNHN F-TAL 4 (posterior-most region of the mandible, only the retroarticular, articular and posterior parts of the surangular and angular) and MNHN F-TAL 7 (almost complete mandible, missing most of the surangular) to create a 'composite specimen' mandible by combining both specimens. Although the use of composite specimens is not always ideal, the holotype of *A. talainti* is too damaged for reliable comparison and morphometric analysis, therefore this composite specimen would be useful, given that it is a phytosaur representing the non-leptosuchomorph Mystriosuchinae clade.

Institutional abbreviations. BSPG, Bayerische Staatssammlung für Paläontologie und Geologie, Munich, Germany; CMNH, Carnegie Museum of Natural History, Pittsburgh, PA, USA; GPIT, Institut und Museum für Geologie und Paläontologie der Universität Tübingen, Germany; ISI, Indian Statistical Institute, Kolkata, India; MB, Museum für Naturkunde, Berlin, Germany; MNHN, Muséum national d'Histoire naturelle, Paris, France; NHMD, National History Museum of Denmark, Copenhagen, Denmark; NHMW, Naturhistorisches Museum Wien, Vienna, Austria; NMMNHS, New Mexico Museum of Natural History and Science, Albuquerque, NM, USA; NOVA-FCT-DCT, Departamento de Ciências da Terra, Faculdade de Ciências e Tecnologias, Universidade NOVA de Lisboa, Lisbon, Portugal; PEFO, Petrified Forest National Park, AZ, USA; SAM-PK, Iziko South African Museum, Cape Town, South Africa; SMNS, Staatliches Museum für Naturkunde, Stuttgart, Germany; TMM, Texas Memorial Museum, Austin, TX, USA; TTU P, Texas Tech University, Lubbock, TX, USA; USNM, National Museum of Natural History, Washington DC, USA; UCMP, University of California Museum of Paleontology, Berkeley, CA, USA; ZMNH, Zhejiang Museum of Natural History, Hangzhou, China; ZPAL, Institute of Paleobiology, Polish Academy of Sciences, Warsaw, Poland.

Geometric morphometrics

Geometric morphometrics was applied to analyse and compare the morphological variation in our sample. The analyses were focused on the lateral view of the posterior region of the mandible, including the surangular, articular, retroarticular, angular, splenial, and the posterior portion of the dentary (dorsal region of the posteriormost five alveoli of the dentary, adjacent to the sutural contact), to ascertain the extension and shape of the external mandibular fenestra as well.

In carrying out the analysis, the software packages tpsUtil v1.82 (Rohlf 2022) and tpsDig2 v2.31 (Rohlf 2017) were used to digitize 13 landmarks and 66 semi-landmarks (Fig. 2) on each specimen (Figs 3–6). All specimens used were from the right hemi-mandibular region. However, given that some specimens were left hemi-mandibles (Figs 3B, C; 4B, D; 5A, E; 6A, B), when necessary the specimens were mirror-imaged because landmark analysis requires all specimens to be equally oriented.

A total of 13 landmarks (Fig. 2) were identified along the surface of the mandible bones and the fenestra edges. These are as follows: (1) the last portion of the dorsal region of the dentary, positioned anterior to the external mandibular fenestra, usually between the fourth and fifth posterior alveoli; (2) dorsal-most extent of the anterior surangular projection, posterior to the region of the dentary–surangular suture (*sensu* López-Rojas *et al.* 2022); (3) dorsal-most extent of the posterior surangular projection, nearly two-thirds of the way along the dorsal length of the surangular (*sensu* López-Rojas *et al.* 2022); (4) posterior region of the surangular, with placement of the landmark in the anterior extent of the glenoid fossa; (5) the posterior reach of the articular (i.e. the posterior-most projection of the articular); (6) the deepest point of the articular–retroarticular concavity, in the posterior region of the mandible; (7) the posterior-most reach of the projection of the retroarticular process; (8) the 'inflection point' (i.e. the point of the ventral region of the angular where the mandible sharply changes direction); if no inflection point is present, this landmark is positioned at the ventral-most extent of the ventral border of the angular in lateral view; (9) the anterior reach of the ventral edge of the mandible (this landmark is positioned on the ventral angular, one alveolus anterior to landmark 1); (10) the anterior-most extent of the external mandibular fenestra; (11) the dorsal

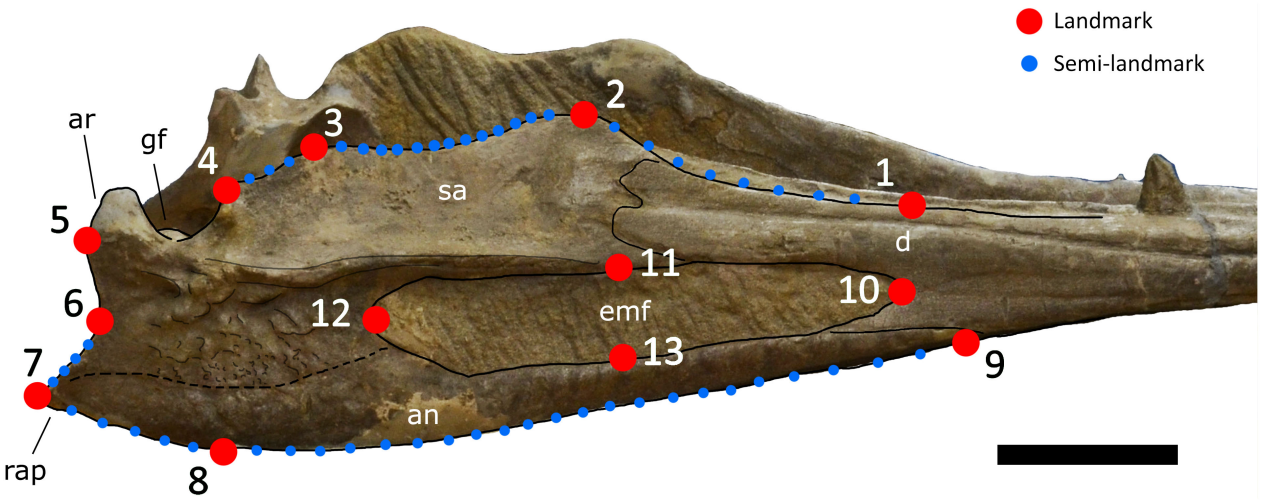

FIG. 2. Landmarks and semi-landmarks placed, as an example, on specimen SMNS 91574, *Mystriosuchus planirostris* (mirror image), in lateral view. See main text for detailed descriptions of landmarks 1–13. Semi-landmarks describe the shape of the: dentary to anterior surangular region (landmarks 1–2; 10 semi-landmarks); shape of the dorsal region of the surangular (landmarks 2–4, 20 semi-landmarks); retroarticular projection (6–7; 6 semi-landmarks); and shape of the ventral region of the angular (7–9; 30 semi-landmarks). *Abbreviations*: an, angular; ar, articular; d, dentary; emf, external mandibular fenestra; gf, glenoid fossa; rap, retroarticular process; sa, surangular. Lines are interpretative drawings of the bone limits and rugosities. Scale bar represents 5 cm.

edge of the external mandibular fenestra, at half the anteroposterior length of the external mandibular fenestra; (12) the posterior-most extent of the external mandibular fenestra; and (13) the ventral edge of the external mandibular fenestra, at half the anteroposterior length of the external mandibular fenestra. Landmarks 10 and 11 should be aligned along the horizontal and vertical axes with 12 and 13, respectively. The landmarks from 1 to 4 were used to obtain the relative proportions of the surangular; those from 5 to 9 were used to obtain the posterior and ventral shapes of the posterior region of the mandible; and those from 10 to 13 were used to determine the shape and proportions (length and height) of the external mandibular fenestra.

In the specimens of *Mystriosuchus planirostris* (SMNS 10260) (Fig. 6C) the retroarticular process is broken posteriorly, therefore landmark 7 (LM7) was placed at a point further away, posterior to the break. In so doing, more complete mandibles of the same species were taken into account. For *My. planirostris* SMNS 10260, specimens SMNS 9900 and SMNS 91574, which are also used in the present study (Fig. 6B, D), were used as references. The specimen *Mystriosuchus alleroq* NHMD 916731 (López-Rojas *et al.* 2022) is missing the posterior region of the dentary and the anterior region of the angular. Given that the anterior border of the external mandibular fenestra is not preserved in this specimen, an approximate position of its corresponding landmark (LM9) was estimated in accordance with the mandibles of other phytosaurs such as *Mystriosuchus planirostris* (SMNS 9900, SMNS 10260 and SMNS 91574; Fig. 6B–D) for *My. alleroq*.

Justification of the use of the semi-landmarks. The semi-landmarks (SMs) were used to capture the morphology of four structures. These shapes were selected because of the morphological variation in these mandibular regions identified in previous research on phytosaurs (Jones & Butler 2018; López-Rojas *et al.* 2022). The four structures are as follows: SM1, the shape of the dorsal surface that goes from the posterior region of the dentary and contacts the anterior dorsal projection of the surangular (10 semi-landmarks from the first to the second landmark); SM2, the shape of the concavity between the first (anterior) and second (posterior) dorsal projection of the surangular (20 semi-landmarks from the second to fourth

FIG. 3. Mandibles with landmarks (red) and the range of positions of the semi-landmarks (blue line). A, *Euparkeria capensis* SAM-PK-5867 (modified from Ezcurra 2016). B, *Diandongosuchus fuyuanensis* ZMNH M8770 (mirror image, modified from Stocker *et al.* 2017). C, *Parasuchus hislopi* ISI R42 (mirror image, modified from Kammerer *et al.* 2016). D, '*Paleorhinus*' cf. *arenaceus* ZPAL Ab III 3592. E, composite specimen of *Angistorhinus talainti* MNHN F-TAL 4 and MNHN F-TAL 7 (Dutuit 1977a). Lines are interpretative drawings of the bone limits. Scale bars represent 5 cm.

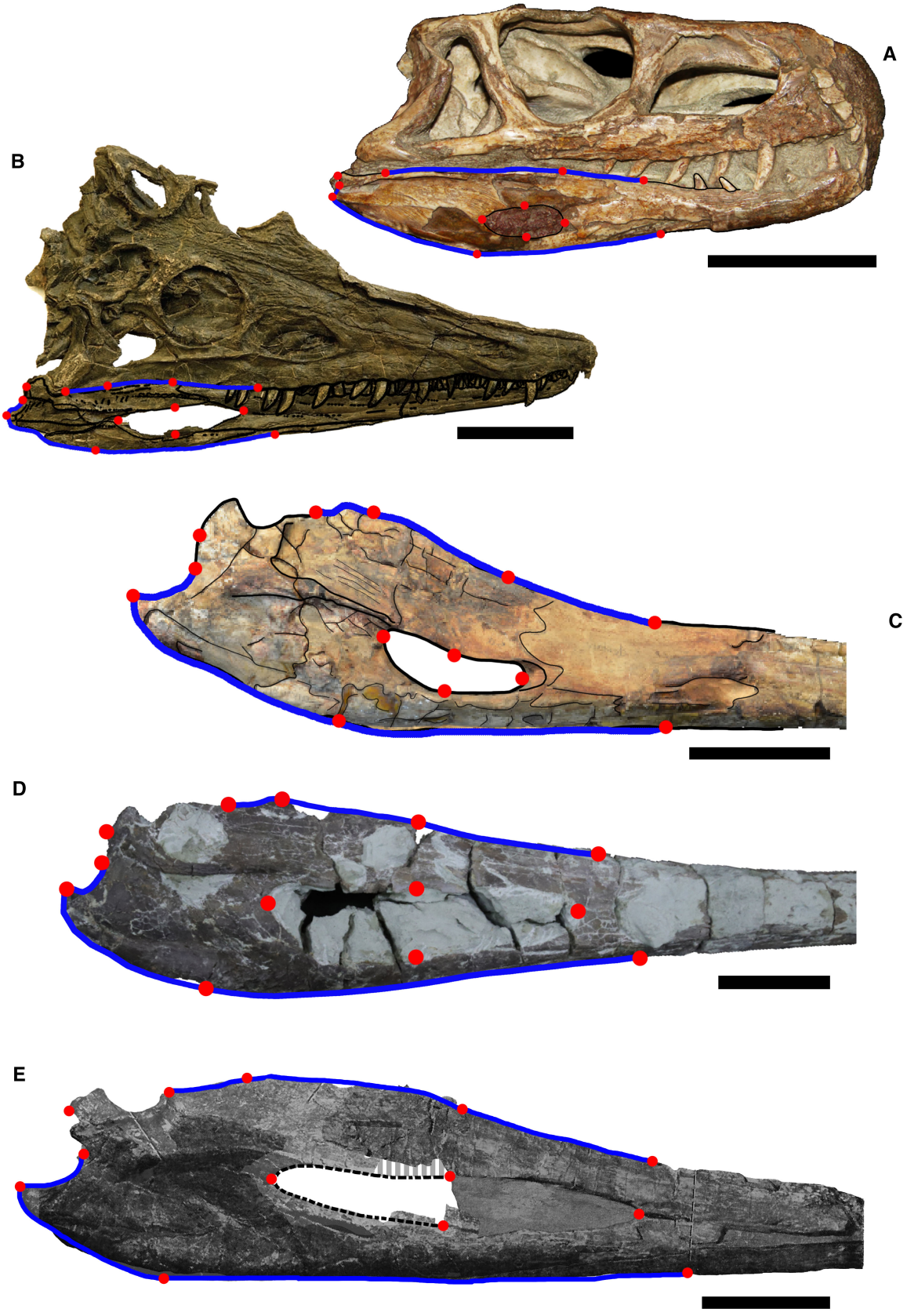

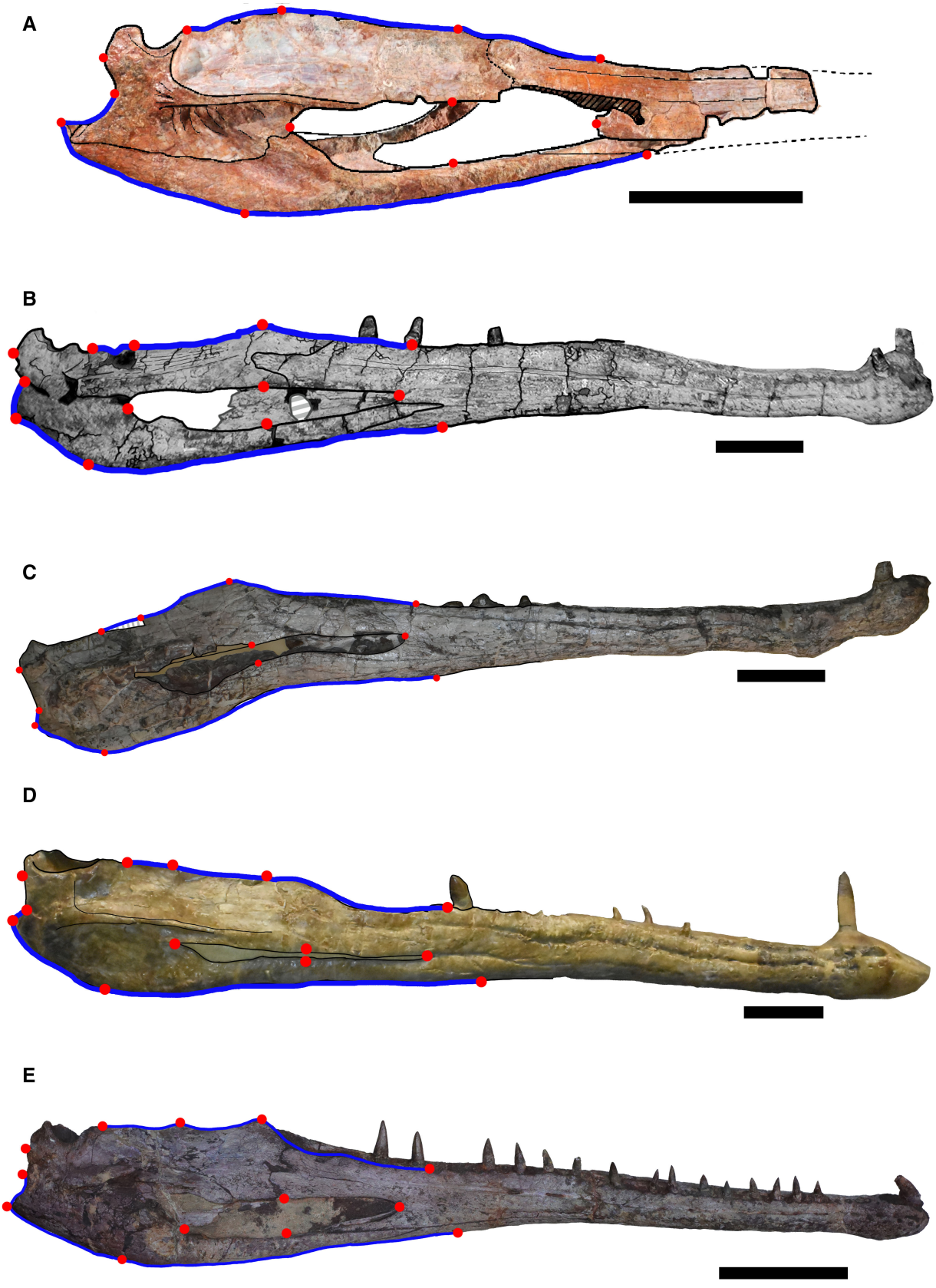

FIG. 4. Mandibles with landmarks (red) and the range of positions of the semi-landmarks (blue line). A, indeterminate phytosaur from the Algarve NOVA-FCT-DCT 5396 (modified from Mateus *et al.* 2014). B, indeterminate specimen NMMNH P-4256 (mirror image, modified from Hunt *et al.* 2006). C, *Smilosuchus gregorii* UCMP A272/27200 (photograph by Marcos Marzola). D, *Smilosuchus adamanensis* UCMP 26699 (photograph by Marcos Marzola). E, *Nicrosaurus kapffi* SMNS 5730. Lines are interpretative drawings of the bone limits. Scale bars represent 10 cm.

landmark); SM3, the shape of the posterior projection of the retroarticular process (six semi-landmarks from the sixth to the seventh landmark); and SM4, the shape of the ventral region of the mandible, from the retroarticular process to an anterior region of the angular (30 semi-landmarks from the sixth to the eighth landmark).

Geometric morphometrics analyses were performed in the RStudio v4.2.2 integrated development environment (RStudio Team 2020). The digitized landmarks and semi-landmarks were then used in a generalized Procrustes analysis (GPA) with the 'gpagen' function from the R-package geomorph (Baken *et al.* 2021; Baken 2023) to rotate, translate and scale each landmark configuration to unit centroid size (CS = the square root of the sum of the squared distance of the landmarks from their centroid; Bookstein 1991). After the GPA, a principal component analysis (PCA) was performed using the 'procSym ()' function from the R-package Morpho (Schlager 2014) to visualize and quantify the morphological variation more easily. The results are presented in the scatterplots and deformation grids (see Results, below). The script used in this analysis was based on the one from Pandolfi *et al.* (2020).

We tested the PCA significance using PCAtest (Camargo 2022, 2024) and pairwiseAdonis (Martinez Arbizu 2020). In both cases the testing was performed first with the specimens alone and then with the specimens enclosed in their major clades (non-Mystriosuchinae, non-Leptosuchomorpha Mystriosuchinae, non-Mystriosuchini Leptosuchomorpha, and Mystriosuchini), as in Jones & Butler (2018).

Phylogenetic analysis

Two phylogenetic analyses were carried out, using TNT v1.6 (Goloboff & Morales 2023) with a modified version of the dataset of Jones & Butler (2018).

First, we ran a maximum parsimony analysis using both the discrete and the landmark and semi-landmark characters (D + L analysis from now on), as in the analysis configuration of Jones & Butler (2018) with its discrete and landmark characters, following Catalano *et al.* (2010) and Goloboff & Catalano (2011). This analysis was undertaken to test the potential taxonomic usefulness of the mandible and the landmarks. To avoid overweighting the contribution of the mandible in our analysis by the duplication of characters, we removed two characters from Jones & Butler (2018), while keeping the rest of the characters equally weighted. Character 77, the dorsal surface of the surangular, is here replaced by landmarks 2–4 and 20 additional semi-landmarks in that region. Character 78, the shape of the retroarticular process in lateral view, is here replaced by landmarks 6 and 7, plus six additional semi-landmarks. In addition to these landmark characters, we introduced a new discrete character regarding the shape of the suture between the dentary and the surangular (see below for explanation of char. 98). Although it was not collected as a landmark character, it was included in the matrix with only discrete characters and was therefore incorporated into the D + L phylogenetic analysis to ensure that no data were omitted.

We followed Jones & Butler (2018) in using the parameters and commands implemented in the analysis for the addition of landmarks in the matrix. We used *lmark rescale* = * to scale the geometric morphometric measurements to unity, *lmark errmarg ()* to accept trees without considering the margin of error, and *bbreak*: *limit 5* to reduce the branch swapping. The aim of these last two commands was to set the parameters to make the process less time-consuming, given that the addition of geometric morphometric data to a matrix makes the analysis computationally heavy.

To test the potential evolutionary signal encoded in the landmark data, a second analysis (termed the 'D analysis') was conducted, in which a phylogenetic analysis was performed by creating discrete characters based on the landmarks. As Jones & Butler (2018) and Holvast *et al.* (2024) indicated, morphometric characters in a phylogenetic matrix entail a heavy and long analysis, taking up to 40 h in the case of one of our D + L analyses. Moreover, the former authors noted that incorporating morphometric data into phylogenetic analysis does not lead to a significant improvement over discrete character-based analyses. For this reason, we modified the discrete-only character matrix of Jones & Butler (2018). This method was adopted to simplify the previous analysis and facilitate the coding and comparison of the taxa. In this discrete phylogenetic analysis (i.e. the D analysis), we modified two of the characters from Jones & Butler (2018) pertaining to the mandible, we added a mandible character from Datta & Ray (2023), and we also created four more. The aim was to enable us to compare the result of the D + L phylogenetic analysis with the D phylogenetic

FIG. 5. Mandibles with landmarks (red) and the range of positions of the semi-landmarks (blue line). North-American Mystriosuchini phytosaurs: A, *Protome batalaria* PEFO 34034 (mirror image, modified from Stocker 2012); B, *Machaeroprosopus buceros* NMMNH P-36051 (modified from Zeigler *et al.* 2003); C, *Machaeroprosopus pristinus* UCMP 27018 (photograph by Marcos Marzola); D, *Machaeroprosopus pristinus* UCMP 7043/27018 (photograph by Marcos Marzola); E, *Machaeroprosopus mccauleyi* UCMP 126999 (mirror image, photograph by Marcos Marzola); F, *Redondasaurus bermani* CMNH 69727 (modified from Rinehart *et al.* 2009). Lines are interpretative drawings of the bone limits; striped fill was used to indicate the gaps due to breakage. Scale bars represent 10 cm.

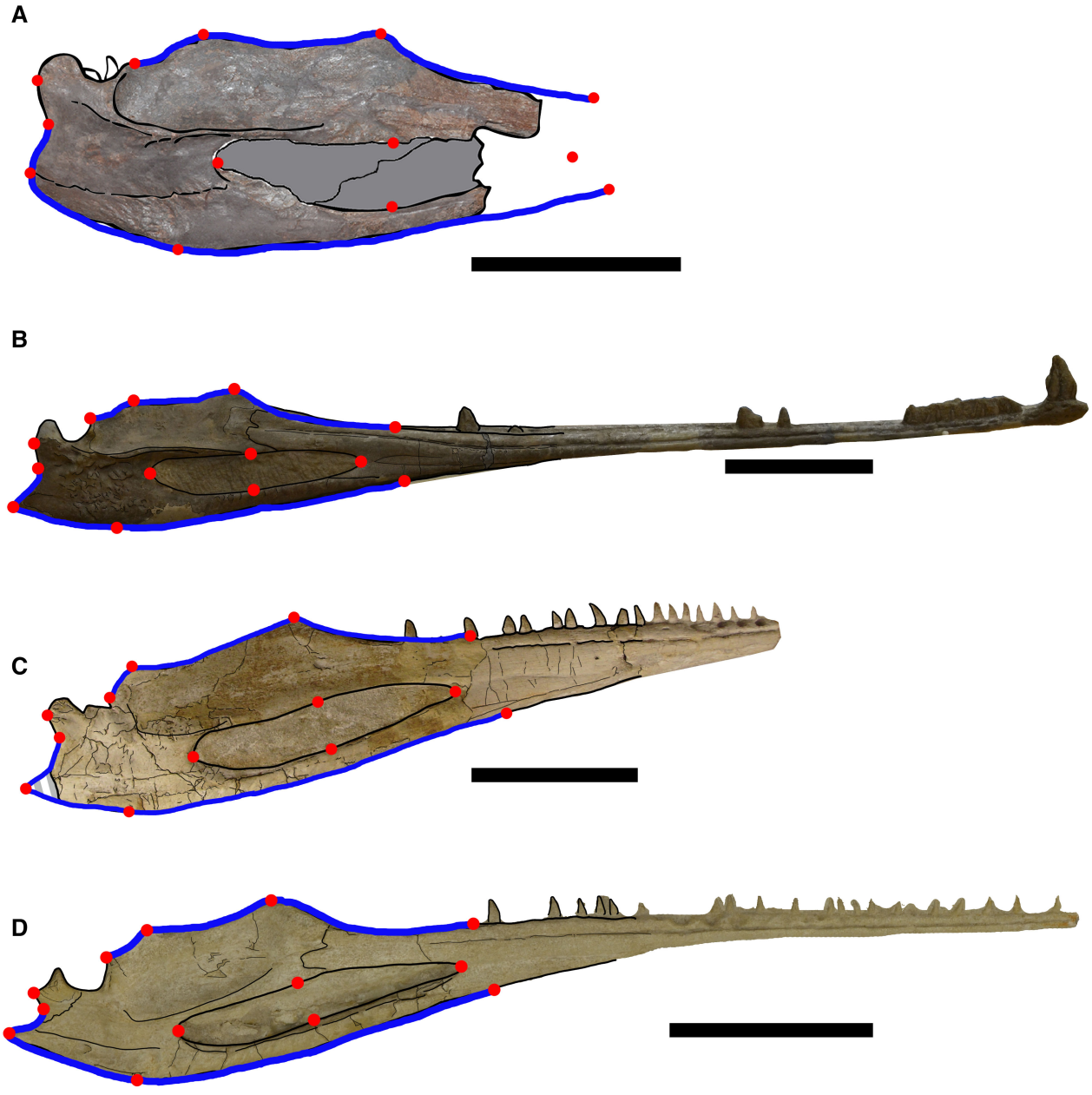

FIG. 6. Mandibles with landmarks (red) and the range of positions of the semi-landmarks (blue line). European Mystriosuchini phytosaurs: A, *Mystriosuchus alleroq* NHMD 916731 (mirror image); B, *Mystriosuchus planirostris* SMNS 91574 (mirror image); C, *Mystriosuchus planirostris* SMNS 10260; D, *Mystriosuchus planirostris* SMNS 9900. Lines are interpretative drawings of the bone limits; dashed lines were used to fill the broken gaps. All scale bars represent 10 cm.

analysis (see Results, below). For an explanation of the characters modified and added to the matrix, see Results.

We analysed this second character matrix using a traditional search analysis (a heuristic search algorithm) of maximum parsimony, with tree bisection reconnection with one random seed, 1000 replications and saving 10 trees per replication. An additional round of tree bisection reconnection using trees from RAM as starting trees was performed after the first analysis.

We introduced *Mystriosuchus steinbergeri* (Butler *et al.* 2019) into the analysis, in place of its specimen number NHMW 1986 0024 0001 from Jones & Butler (2018). We also added the specimen *Mystriosuchus alleroq* NHMD 916731 from López-Rojas *et al.* (2022). Even though '*Paleorhinus*' cf. *arenaceus* (Dzik & Sulej 2007) has previously been used for morphometric analysis, this material is currently undergoing a systematic revision and was therefore not included in our phylogenetic analyses. We removed most of the unnamed terminal taxa (MB.R. 2747, NMMNHS P-31094, NMMNHS P-4781, PEFO 34852, TMM 31100 1332, USNM v 17 098, USNM v 21 376). The removal of these taxa from Jones & Butler (2018) was either because we were not able to access these taxa first-hand or because some of these specimens did not preserve the mandible.

For each analysis, we ran two different datasets, one including only formally named taxa, and a second one adding two unnamed specimens of particular interest for this study (NOVA-FCT-DCT 5396 and NMMNHS P-4256). This resulted in a total of four analyses: D + L1, D + L2, D1 and D2.

RESULTS

The first two principal components obtained in the PCA accounted for 58.73% of the total variance in the lateral view of the mandibles of the phytosaur sample. The relationship between the first two principal components (PC1 33.45% and PC2 25.28%) is represented in Figure 7. In both PC significance analyses, the PCA yielded no significant results (Appendix S1, Rmd file). However, these results may be affected by the low sample size, making it difficult to discern variation among species and clades. Despite the lack of significance in the PCA results, variation in the shape and morphology of the lateral side of the mandible is observed, which may be relevant for phylogenetic analysis.

The PC1 values (Fig. 7, *y* axis) are associated with the length, shape and curvature of the dorsal region of the surangular (LM1–4) and of the ventral region of the angular (LM7–9). The position of LM8 (Fig. 2) indicates where the inflection point of the angular is, which is where the ventral region of the angular changes its direction. Positive PC1 values are associated with more deeply nested phytosaurs from the clade Leptosuchomorpha (*Smilosuchus*, *Protome*, *Machaeroprosopus*, *Redondasaurus* and *Mystriosuchus*), whereas the negative PC1 values are associated with more basal phytosaurs (*Diandongosuchus*, *Angistorhinus* and *Parasuchus*). Both the NOVA-FCT-DCT 5396 and NMMNHS P-4256 specimens, the leptosuchomorph *Smilosuchus gregorii* and the outgroup (*Euparkeria*) also plot in the negative PC1 region.

The PC2 values (Fig. 7, *y* axis) are found to be related to the difference in height of the post-dentary bones relative to the height of the dentary. For negative PC2 values, the taxa have a greater height between the dorsal-most region of the surangular and the ventral-most border of the angular relative to the dentary height. This is reflected in stouter and higher post-dentary bones. The taxa with these negative values are *Parasuchus hislopi* (ISI R42), '*Paleorhinus*' cf. *arenaceus* (ZPAL Ab III 3592), *Mystriosuchus alleroq* (NHMD 916731), *Machaeroprosopus pristinus* (UCMP 27018 and UCMP 7043/27018), *Ma. buceros* (NMMNHS P-36051), *Redondasaurus bermani* (CMNH 69727) and the specimen NOVA-FCT-DCT 5396. In contrast, taxa with positive PC2 values have an anteroposteriorly elongated and thickened post-dentary region, with a dorsoventral height comparable to that of the dentary. These taxa are *Smilosuchus gregorii* (UCMP A272/27200) and *S. adamanensis* (UCMP 26699), *Nicrosaurus kapffi* (SMNS 5730), *Mystriosuchus planirostris* (SMNS 91574, 9900, 10260), *Protome batalaria* (PEFO 34034), *Machaeroprosopus mccauleyi* (UCMP 126999), *Angistorhinus talainti* (composite specimen MNHN F-TAL4–7), *Diandongosuchus* ZMNH M8770, the specimen NMMNHS P-4256, and the outgroup *Euparkeria*.

According to the PCA analysis, both PC1 and PC2 (Fig. 7) recover relationships between the length and height of the external mandibular fenestra. This relationship was characterized by Datta & Ray (2023), who measured the external mandibular fenestra based on how long it was relative to the height, and described it as short (in *Euparkeria*), moderately long (in *Diandongosuchus* and *Parasuchus*), or greatly elongated (in Mystriosuchinae phytosaurs). However, regarding the height of this fenestra, it was not discussed further.

It is noteworthy that PC1 and PC2 do group the taxonomically related forms, even though the results are not significant. Despite PCA not being a reliable method for inferring evolutionary trends (Uyeda *et al.* 2015 and references within), the results show that the landmark data analysed may have evolutionary significance. To test this hypothesis, we ran a phylogenetic analysis with a matrix composed of discrete and landmark characters (D + L characters), following Jones & Butler (2018). The consensus tree resulting from this analysis (see Results, below)

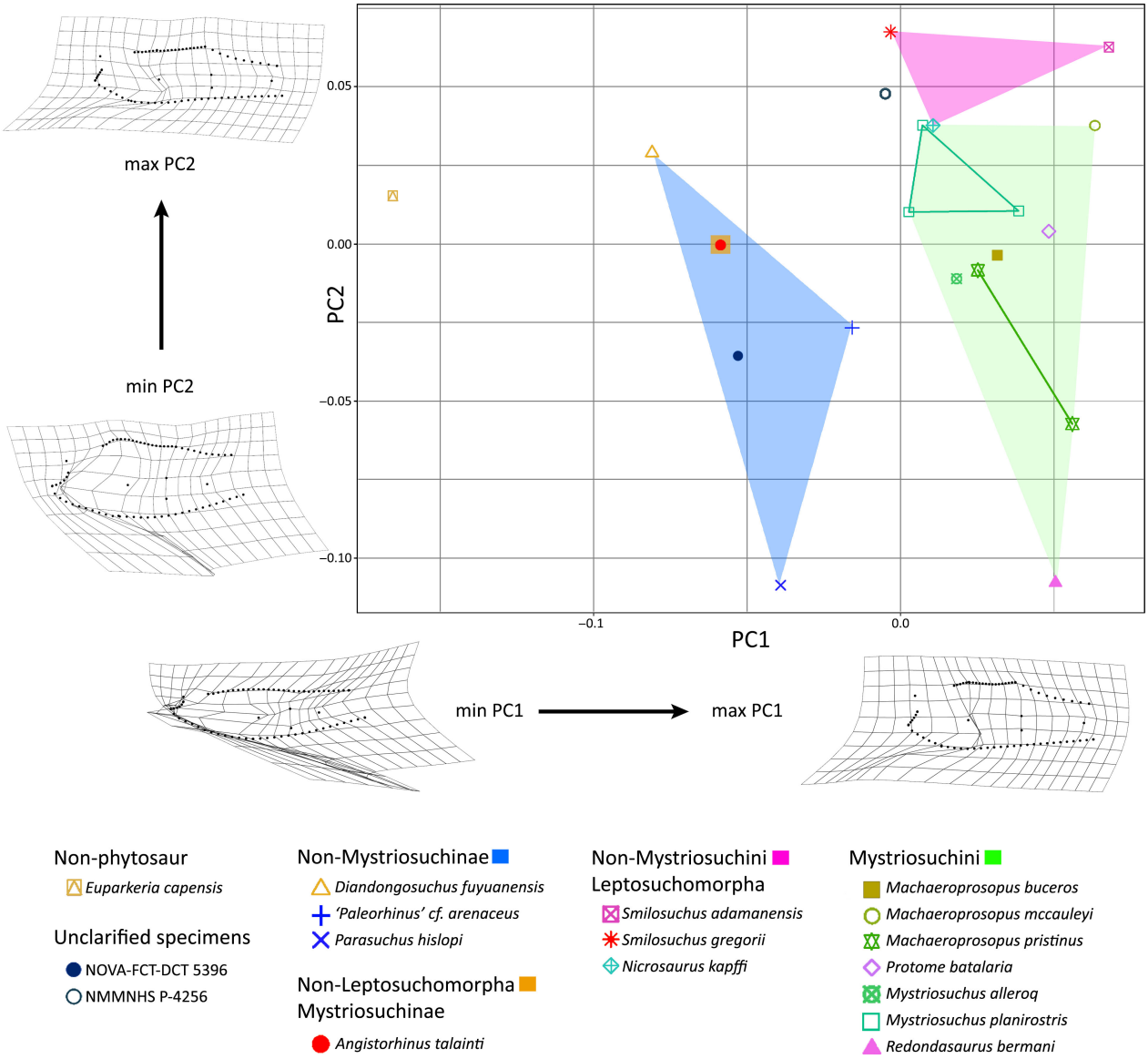

FIG. 7. Scatterplot of the principal component analysis for principal component (PC)1 and PC2. The deformation grids of the lateral mandible of phytosaurs with minimum and maximum PC1 and PC2 values are shown next to the respective axis. The different clade regions of the graph were added manually.

has a similar topology to that of Jones & Butler (2018), even with the influence of the morphometrics in the posterior region of the mandible.

We modified the character 'dorsal surface of surangular' (char. 77 in Jones & Butler 2018; we maintain the same number). This character was originally described with two states: gently convex (state 0), or gently concave rising to apex just posterior to dentary contact (state 1). Here, we found that the shape of the dorsal surangular surface differs more among phytosaurs. Ló pez-Rojas *et al.* (2022) described this region in greater detail, indicating that in some species, including the ones belonging to *Mystriosuchus* or *Protome*, the surangular has two dorsal projections (an anterior and a posterior one), with a concavity between them. However, there are other species with only a posterior projection of the surangular, as in *Angistorhinus talainti* (composite specimen MNHN F-TAL 4–7), *Machaeroprosopus mccauleyi* (UCMP 126999), and *Ma. pristinus* (UCMP 27018). Therefore, we rephrased the character and added the following: straight or slightly convex surface, no dorsal projections of the surangular (state 0); only a posterior projection of the surangular (state 1); both an anterior and a posterior projection of the surangular, with a marked concavity between them (state 2).

We also modified the character 'shape of the retroarticular process in lateral view' (char. 78 in Jones & Butler 2018; we maintain the same number). This character was originally described with two states: distally sharply pointed or curved into a posterodorsally oriented hook (state 0), or distally rounded or blunt (state 1). However, we found that the retroarticular region, in the specimens with a blunt region, could be differentiated into two. We rephrased state 1 from Jones & Butler (2018) to read: distally rounded, projected posteriorly (state 1); and distally round or blunt, but not projected (state 2). This differentiation is needed because in species such as *Protome batalaria* or *Machaeroprosopus buceros* the retroarticular process is round and projected, but not hook-like (Fig. 5A, B). This contrasts with *Ma. mccauleyi* (UCMP 126999) (Fig. 5E) or the specimen NMMNHS P-4256 (Fig. 4B), in which the retroarticular region is blunt and not projected.

We added, without any additional changes, the character 'shape, in terms of length, of the external mandibular fenestra' from Datta & Ray (2023), here coded as character 96. However, we introduced a new character regarding the shape of the external mandibular fenestra, specifically in terms of its height (char. 97). The ratio in question is calculated by dividing the height of the fenestra (emfH) by the total height of the mandible (mT) from the angular ventral-most border to the surangular dorsal-most border. This ratio indicates how much height the fenestra opening occupies in the mandible; it could be an opening greater than 20% of the total height (state 0), or a short opening, smaller than 20% (state 1). State 1 is exclusive to the specimens of *Smilosuchus* here studied (*S. adamanensis* and *S. gregorii*), with openings ranging from 10% to 15% of the total height of the mandible, whereas other species (such as *Angistorhinus*, *Mystriosuchus* or even the oldest phytosaur, *Diandongosuchus*) have between 20% and 30%.

We also included the new character 98 regarding the 'suture between the dentary and the surangular', following Stocker (2012). Stocker (2012) provided a morphological description of how, in *Protome batalaria*, the boundary of the dentary extends as two prongs into the surangular, although this was not applied in a phylogenetic analysis. These two prongs can be found in other species such as *Mystriosuchus planirostris*, *My. alleroq* or *Nicrosaurus kapffi*. However, there are species that present a blunter suture between the dentary and surangular, such as *Diandongosuchus fuyuanensis*, *Parasuchus hislopi* and *A. talainti*. Likewise, there are species that present only one prong, instead of two, from the dentary into the surangular, as in *Smilosuchus gregorii* and *S. adamanensis*, and the specimen NMMNHS P-4259. To describe this feature, therefore, we created the states of blunt, perpendicular to the horizontal plane (state 0); singular prong wedging from the dentary into the surangular (state 1); or double prong from the dentary into the surangular (state 2).

The new character 99, 'dorsal transition of the dentary to the surangular', was added because the PC1 scores (Fig. 7) showed that the angle between the dentary and the surangular varies among species. The dorsal edge could range from an almost flat transition at an angle of less than 10° (state 0); to an angle of curvature between 10° and 20° (state 1); to a more tilted angle between 20° and 30° (state 2); or a strong curvature of over 30° (state 3).

Last, we also included the new character 100, 'angular ventral curvature', based on the PC1 scores (Fig. 7). The inflection point (i.e. LM8) was used to mark the difference between the posterior-most and the ventral portions of the angular. In some species there is a gentle curvature from the retroarticular region through the entire angular (state 0), whereas in other specie, there is a distinct point of inflection between the posterior-most angular and the ventral region of the angular (state 1).

After adding these characters, we ran a TNT analysis and obtained a strict consensus cladogram of six most parsimonious trees (MPTs; Fig. 8B) from dataset D1 (which includes only the named species). The tree length was 346, with a consistency index (CI) of 0.425 and a retention index (RI) of 0.668. From dataset D2 (adding the two phylogenetic unresolved specimens), we recovered 189 MPTs (see Discussion, below), with 352 steps as the best score tree length, and a CI of 0.418 and an RI of 0.675.

In the D1 phylogenetic analysis (Fig. 8B), the node of the clade Leptosuchomorpha was characterized by three of the new and modified mandible characters as synapomorphies. Character 77 was modified from Jones & Butler (2018) after the landmark phylogenetic analysis, given that the dorsal surangular shape was originally described as having either a gentle convexity or concavity. In our results, this character (shape of the dorsal surangular) changed from exhibiting only a posterior projection on the dorsal surangular (state 1) to having both anterior and posterior projections in the dorsal surangular, with a marked concavity between them (state 2) in leptosuchomorph phytosaurs. Among the newly added characters, character 98 (suture between dentary and surangular) exhibits a perpendicular, blunt contact between these bones in non-leptosuchomorph phytosaurs (state 0), whereas leptosuchomorph phytosaurs present a double-pronged suture from the dentary to the surangular (state 2); and character 99 (dorsal transition from dentary to the surangular), is represented in non-leptosuchomorph species by a gentle curvature between 10° and 20° (state 1), while leptosuchomorph phytosaurs have a curvature higher than 20° (states 2–3).

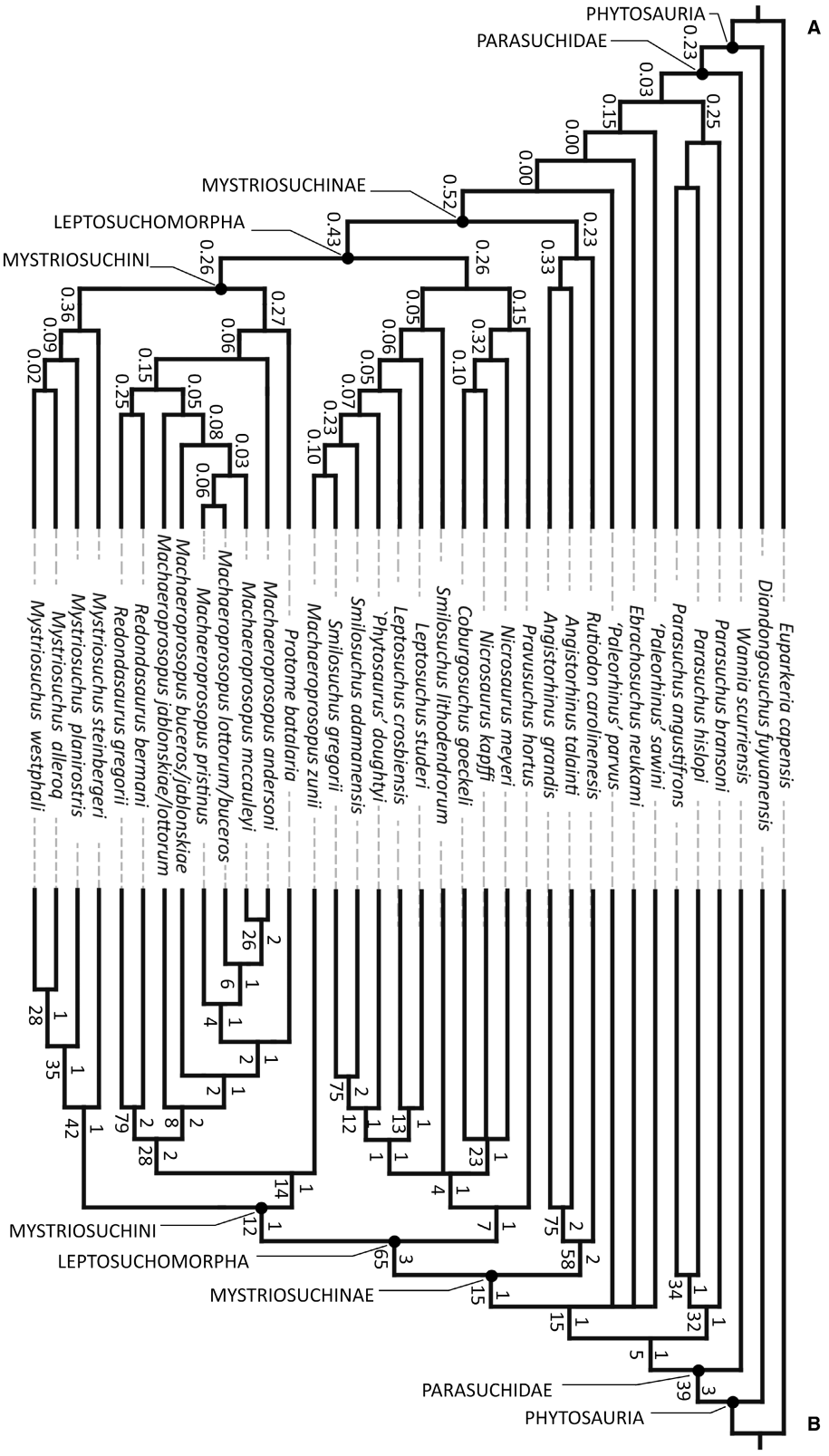

FIG. 8. Phylogenetic analyses from the dataset without the addition of indeterminate specimens. A, most parsimonious tree (MPT) from the analysis of discrete and landmark (D + L1) characters. B, consensus tree of the six MPTs, from only the discrete analysis with the update of the discrete characters 77 and 78, and the addition of the new discrete characters 96–100 (D1).

It is important to note the general low branch support observed in both landmark-based analyses. During several iterations of the dataset, we observed that minimal modification of the location of landmarks and semi-landmarks, despite not altering the general structure of the tree, may affect the placement of some terminal taxa. Notably, small mistakes and typographical errors in the landmark values resulted in doubling and tripling of the computing time needed to obtain a topology.

DISCUSSION

The most important finding is a separation between the Leptosuchomorpha phytosaurs (*Protome*, *Smilosuchus*, *Nicrosaurus*, *Machaeroprosopus* and *Mystriosuchus*), which had PC1 values that were positive or very close to positive, and the non-Leptosuchomorpha phytosaurs (*Angistorhinus*, *Parasuchus*, '*Paleorhinus*' and *Diandongosuchus*), along with the outgroup (*Euparkeria*), which had more negative PC1 values. Although this separation was not statistically significant (p-values ranged between 0.1 and 0.6), it may have been influenced by the limited sample size, given that our analyses included only 14 phytosaur species out of nearly 40 known species. However, a non-significant statistical result does not necessarily indicate the absence of phylogenetic differences between the mandibles. The introduction of these morphometric data as characters for the D + L datasets, and later as discrete characters for the D datasets, shows that the mandibles present important phylogenetic data.

The D + L1 phylogenetic analysis (Fig. 8A) recovers a clear separation of the non-Mystriosuchini Leptosuchomorpha into two monophyletic clades: European taxa (*Nicrosaurus* and *Coburgosuchus*) with *Pravusuchus hortus* Stocker 2010, and the North American *Smilosuchus*–*Leptosuchus* clade. In contrast to the D1 dataset (Fig. 8B), although these two main clades are differentiated but in a polytomy with *Smilosuchus lithodendrorum*, the species *Pravusuchus hortus* was recovered as the basal-most non-Mystriosuchini leptosuchomorph taxon outside these clades. Stocker (2010) originally recovered *Pravusuchus* within Mystriosuchini, suggesting a close relationship with *Mystriosuchus* and *Machaeroprosopus*. However, later phylogenetic analyses by Jones & Butler (2018) recovered it closer to *Nicrosaurus* and *Coburgosuchus*, as in our D + L1 analysis. Despite these shifts, the position of *Pravusuchus* as a non-Mystriosuchini leptosuchomorph remains consistent with previous research.

Another surprising result in the non-Mystriosuchini Leptosuchomorpha clade is the different position of *Machaeroprosopus zunii* in the D + L1 vs D1 datasets. We explored the possibility of recovering *Ma. zunii* as a non-Mystriosuchini leptosuchomorph. We ran a constrained analysis on TNT, and repeated the search for the MPTs, recovering 522 MPTs of 347 steps. Despite the general lack of resolution, in which both Mystriosuchini and the non-Mystriosuchini Leptosuchomorpha were recovered as large polytomies, it requires only one additional step to recover *Machaeroprosopus zunii* as a non-Mystriosuchini leptosuchomorph, as was the case in the D + L1 analysis (Fig. 8A).

One difference between these two analyses is also the position of *Protome batalaria*. This species was recovered either as the basal-most taxon of the *Machaeroprosopus*–*Redondasaurus* clade (D + L1 analysis) or deeply nested within the *Machaeroprosopus* clade (D1 analysis). The phylogenetic position of *P. batalaria* was first shown as located within Leptosuchomorpha by Stocker (2012) based on the shape of its quadratojugal. However, in the analyses carried out by Jones & Butler (2018), *P. batalaria* was also recovered as part of Mystriosuchini, as one of the basal-most taxa of *Machaeroprosopus*. Regardless of the analytical approach used (D + L1 or D1), the mystriosuchin affinities of *P. batalaria* are supported by the new data. This result reinforces the mystriosuchin position, as well as the Jones & Butler (2018) result, while it challenges the use of isolated squamosals to assign partial skulls to either Mystriosuchini or non-Mystriosuchini leptosuchomorphs (Long & Murry 1995; Parker & Irmis 2006). However, the scope of the present research refers only to the usefulness of the mandible to assign partial mandibles (similarly to the usefulness of the squamosal as suggested by previous research on partial skulls). As indicated by Jones & Butler (2018), future research should focus on other dorsal skull regions, such as the presence or absence of parietal prongs to establish better differentiation among leptosuchomorph phytosaurs.

The main difference between the results of the D + L1 and D1 trees (Fig. 8) is the internal organization of the *Machaeroprosopus* clade. These internal relationships within *Machaeroprosopus* have been discussed at length in the literature (e.g. Zeigler *et al.* 2002; Hungerbühler *et al.* 2013), and Jones & Butler (2018) provide a better resolution by adding the landmark characters.

Despite these differences between the two analyses (Fig. 8), the D1 analysis recovered some mandible characters as synapomorphies for the clade Leptosuchomorpha. One of these is the concavity between the anterior and posterior projections of the dorsal region of the surangular (char. 77:2). This condition is present in Leptosuchomorpha phytosaurs such as *Mystriosuchus*, *Machaeroprosopus*, *Protome* and *Nicrosaurus*, whereas *Smilosuchus* presents a reversion to state 0 (straight, no dorsal projections of the surangular). In the case of the non-Leptosuchomorpha phytosaurs (i.e. the taxa with negative PC1 values; Fig. 7) the shape of the dorsal region of the surangular is straight, slightly concave dorsally (state 0).

The double-prong suture between the dentary and the surangular (char. 98:2) is present in leptosuchomorph phytosaurs, such as *Nicrosaurus*, *Protome*, *Mystriosuchus* and some *Machaeroprosopus*. In non-Leptosuchomorpha phytosaurs, such as *Angistorhinus* (composite specimen MNHN F-TAL 4–7; Fig. 4A) or *Parasuchus* (ISI R42; Fig. 3C), the suture between the dentary and surangular is blunter (state 0 of the character). This difference is also observed in other non-Leptosuchomorpha species that were not included in this study because the mandibles were too incomplete, such as *Colossosuchus* (Datta & Ray 2023) from India. State 2 is found in the non-Mystriosuchini Leptosuchomorpha phytosaurs *Nicrosaurus kapffi* SMNS 5730 (Fig. 4E; Hungerbühler 1998), but mostly in mystriosuchin phytosaurs, such as *Protome batalaria* PEFO 34034 (Fig. 5A) (Stocker 2012), *Mystriosuchus alleroq* NHMD 916731 (Fig. 6A) (López-Rojas *et al.* 2022), *My. planirostris* (Fig. 6B) (SMNS 91574), and *Machaeroprosopus buceros* NMMNHS P-36051 (Fig. 5B) (Zeigler *et al.* 2003). However, this double-pronged articulation is not found in the non-Mystriosuchini leptosuchomorph species *Smilosuchus* (UCMP 26699, UCMP A272/27200; Fig. 4C–D) (Zeigler *et al.* 2003; Hunt *et al.* 2006). In fact, *Smilosuchus* shows only a single prong that wedges into the surangular (state 1 of the character). '*Paleorhinus*' cf. *arenaceus* (ZPAL Ab III 3592) seems to have this double-pronged articulation (Fig. 3D), but the mandible is partly broken and covered with sediment. We therefore refrain from describing it as having a double-pronged articulation between the dentary and the surangular in this study.

Our phylogenetic analysis also recovers the transition between the dorsal region of the dentary–surangular (char. 99) as a synapomorphy of Leptosuchomorpha. Non-Leptosuchomorpha Mystriosuchinae show a slight inclination between 10° and 20° (state 1), whereas leptosuchomorphs always have a transition greater than 20° (states 2 and 3). Nevertheless, the lack of data and the taphonomic distortion in some leptosuchomorph specimens (*Smilosuchus adamanensis* UCMP 26699; Fig. 4C) make it impossible to determine which state represents the synapomorphic condition of the clade.

Apart from these synapomorphic characters of Leptosuchomorpha phytosaurs, additional characteristics of the mandible are found that have a lesser influence on phylogenetics. In the present analysis, we found that the height itself could be an autapomorphy of *Smilosuchus* (*S. adamanensis* UCMP 26699 and *S. gregorii* UCMP A272/27200), given that these species have an opening with a low height in comparison with other phytosaurs. (char. 97:1). However, the phylogenetic analysis did not recover this state as an autapomorphy of *Smilosuchus* clade, given that there are other species that were not coded in the present analysis, and it may influence it.

Phylogenetic clarification of the Iberian & North American specimens

The use of geometric morphometrics in a phylogenetic framework has primarily been conducted in mammals and dinosaurs, achieving positive results in differentiating the species, with an accuracy of nearly 80% in most cases (Maiorino *et al.* 2013; Jansky *et al.* 2016). For phytosaurs, Jones & Butler (2018) incorporated landmark-based data into their phylogenetic analysis to improve the resolution of poorly supported nodes, such as *Machaeroprosopus* or *Smilosuchus*. In the present research we expand this previous research by adding three landmark-based characters in the region posterior to the dentary in mandibles. This new phylogenetic framework is used here to test the taxonomic affinities of the specimens NOVA-FCT-DCT 5396 and NMMNHS P-4256 (Fig. 9).

Position of the Iberian phytosaur NOVA-FCT-DCT 5396. - The PC1 datapoint places NOVA-FCT-DCT 5396 in the same region as the non-Leptosuchomorpha phytosaurs *Angistorhinus* (*A. talainti* composite specimen MNHN F-TAL 4–7), *Parasuchus hislopi* (ISI R42) and '*Paleorhinus*' cf. *arenaceus* (ZPAL Ab III 3592). If we consider the negative PC2 values, it appears in the morphospace of the non-Mystriosuchinae phytosaurs *Parasuchus* and '*Paleorhinus*'.

Overall, the surangular shape of the Iberian phytosaur is closer in shape to *Angistorhinus talainti* (composite specimen MNHN F-TAL 4–7), *Parasuchus* (ISI R42) and '*Paleorhinus*' (ZPAL Ab III 3592), with negative PC1 values, representing a straighter anterior region of the surangular, than to Leptosuchomorpha phytosaurs. Unlike in Leptosuchomorpha phytosaurs, the surangular in NOVA-FCT-DCT 5396 does not present any concavity in its dorsal region (e.g. Figs 4–6). The surangular reaches its greatest height slightly posterior to the posterior border of the external mandibular fenestra, something that is similar to *Angistorhinus talainti*.

NOVA-FCT-DCT 5396 has a marked convexity in the posterior region of the angular. This is reflected by its inflection point (LM8), which is positioned posteriorly to the posterior border of the external mandibular fenestra. In contrast, the PC2 value of '*Paleorhinus*' is closer to positive than that of NOVA-FCT-DCT 5396, representing a gentler curvature of the ventral region of the angular, while *A. talainti* occupies the most positive position relative to NOVA-FCT-DCT 5396, with a PC2 value of zero. The retroarticular process of NOVA-FCT-DCT 5396 bears a similar sharp, posterodorsally projected hook, which resembles the complete retroarticular process of *Angistorhinus talainti* MNHN F-TAL 7, as well as that in the non-Mystriosuchinae phytosaurs *Parasuchus* and '*Paleorhinus*'.

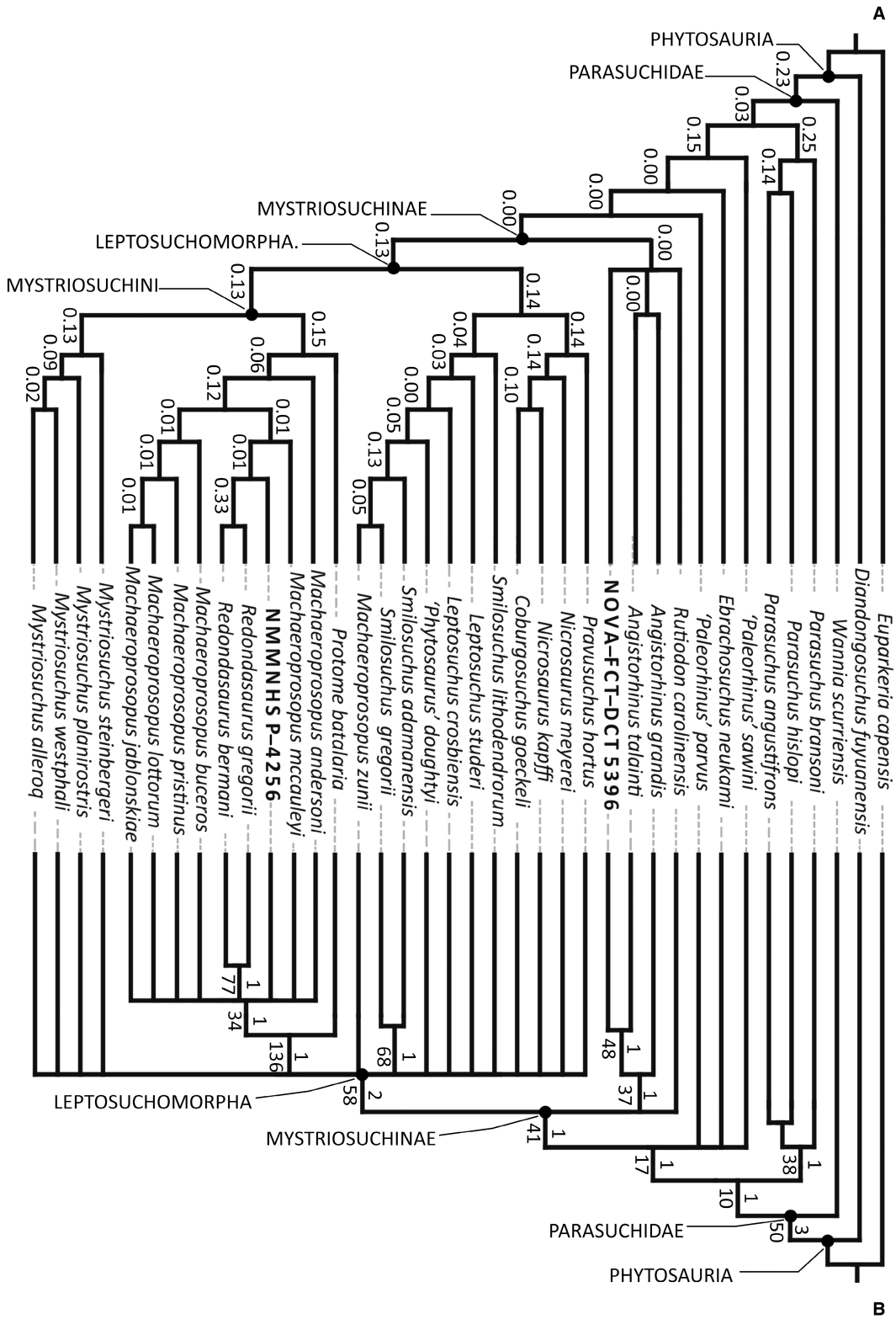

FIG. 9. Phylogenetic analyses from the dataset with the addition of NOVA-FCT-DCT 5396 and NMMNHS P-4256. A, most parsimonious trees (MPTs) from the analysis of discrete and landmark characters (D + L2). B, consensus tree from the 189 MPTs, from only the discrete analysis with the update of the discrete characters 77 and 78, and the addition of the new discrete characters 96–100 (D2).

Based on the PC scores alone, NOVA-FCT-DCT 5396 shows an affinity with the non-Leptosuchomorpha phytosaurs. This is consistent with the late Carnian to Norian period suggested for the Penina locality. Most non-Leptosuchomorpha phytosaurs (*Angistorhinus*, *Ebrachosuchus*, *Parasuchus* or '*Paleorhinus*') are from the late Carnian or early Norian age (Long & Murry 1995; Kammerer *et al.* 2016). The age of the Penina locality in the Silves Group (Algarve Basin), where the specimen was collected, could range from the late Carnian to the Norian according to the vertebrate biostratigraphy (Brusatte *et al.* 2015) and the palynological data (Vilas-Boas *et al.* 2024). Brusatte *et al.* (2015) noted that the Penina locality shares similar sedimentary units and faunal assemblages (mostly consisting of temnospondyls and early archosaurs), to those described by Dutuit (1977a, 1977b) in Morocco and by Dzik (2001) in Poland.

The hypothesis that NOVA-FCT-DCT 5396 is a non-Leptosuchomorpha phytosaur is supported by both phylogenetic results (Fig. 9). In both analyses (D + L and D), NOVA-FCT-DCT 5396 is nested among *Angistorhinus* taxa, showing a close relationship with *Angistorhinus talainti* (the phytosaur from the Argana Basin, Morocco; Dutuit 1977b) in the D analysis (Fig. 9B), while in a polytomy in the D + L analysis (Fig. 9A). The character shared (in the D dataset) by both *A. talainti* and NOVA-FCT-DCT 5396, which distinguishes them from *A. grandis*, is the dorsal shape of the surangular, with only a posterior dorsal projection (char. 77:1). Nonetheless, the shape and morphology of the hook-like retroarticular process also differs from the less marked hooked process of *A. grandis*.

Although no skull material was found for the NOVA-FCT-DCT 5396 specimen, in contrast to *A. talainti*, the new mandible characters enabled us to relate it to the Moroccan phytosaur. In fact, only seven out of 100 phylogenetic characters were coded for the D2 analysis for NOVA-FCT-DCT 5396; these were the new mandible characters, which enabled it to be located in the *Angistorhinus* genus.

Despite this difference, we define the specimen NOVA-FCT-DCT 5396 as *Angistorhinus* cf. *talainti*.

Position of the North American specimen NMMNHS P-4256. In the present analysis, specimen NMMNHS P-4256 appears near the group with positive PC1 values, grouping it with Leptosuchomorpha phytosaurs such as *Smilosuchus*, *Mystriosuchus*, *Redondasaurus* and *Machaeroprosopus* (Fig. 7). NMMNHS P-4256 shares with them a similar angle in the transition between the dentary and the surangular, as found in *Smilosuchus adamanensis* (UCMP 26699), *Redondasaurus bermani* (CMNH 69727) and *Machaeroprosopus buceros* (NMMNHS P-36051).

The dorsal surface of the surangular is slightly concave, with small anterior and posterior projections of the surangular, as in *Protome batalaria* (Fig. 5A) and *Ma. mccauleyi* (Fig. 5E). However, these dorsal projections of the surangular, and the concavity between them, are not as marked as in other phytosaurs such as in *Redondasaurus bermani* (Fig. 5F), *Mystriosuchus alleroq* (Fig. 6A) or *My. planirostris* (Fig. 6B). In fact, the concavity in NMMNHS P-4256 is longer rather than deep, as in *Ma. mccauleyi* (Fig. 5E).

The shape of the external mandibular fenestra in NMMNHS P-4256, following Datta & Ray (2023) is extremely anteroposteriorly long, as in all Leptosuchomorpha phytosaurs (*Smilosuchus*, *Machaeroprosopus* and *Mystriosuchus*). This long fenestra morphology is also reflected in the positive PC1 values (Fig. 7). Regarding the height of the fenestra, however, NMMNHS P-4256 has an opening higher than *Smilosuchus*, and more similar to Mystriosuchini phytosaurs, such as *Machaeroprosopus* or *Mystriosuchus* but longer than the later-diverging taxon *Redondasaurus bermani*.

The point of inflection (LM8) is similarly positioned with respect to *Machaeroprosopus mccauleyi* (UCMP 126999). This inflection point marks a strong convexity between the posterior and the ventral regions of the angular, a feature also observed in *Mystriosuchus planirostris* (SMNS 91574, Fig. 6B). This contrasts with the smooth ventral surface observed in other specimens such as *Machaeroprosopus buceros* (NMMNHS P-36051, Fig. 5B) and *Protome batalaria* (PEFO 34034, Fig. 5A).

Even though there were more specimens from *Machaeroprosopus* than from *Redondasaurus* with which to analyse and compare the specimen, the D + L phylogenetic analysis (Fig. 9A) placed NMMNHS P-4256 as nested with *Machaeroprosopus mccauleyi* and *Redondasaurus*, whereas the D analysis (Fig. 9B) placed it in a polytomy of *Machaeroprosopus* and *Redondasaurus*. Both results are close to previous results obtained by Jones & Butler (2018), reflecting the strong relationship of this specimen with *Machaeroprosopus* taxa, which also aligns with the interpretation by Hunt *et al.* (2006). Also, the dorsal shape of NMMNHS P-4256 more closely resembles that of *Machaeroprosopus* (Fig. 5D, E). In contrast, the strong twin projections of *Redondasaurus bermani* are more similar in shape to those of the genus *Mystriosuchus*. Accordingly, we suggest that specimen NMMNHS P-4256 is cf. *Machaeroprosopus*.

CONCLUSION

Here, we present a 2D landmark-based geometric morphometric analysis of the post-dentary bones of phytosaur mandibles for phylogenetic character identification. This approach led to the revision of two mandibular characters from Jones & Butler (2018) and the introduction of four novel characters. The addition of these characters

highlighted three synapomorphic features in the mandible that are characteristic of Leptosuchomorpha phytosaurs: dorsal surface of the surangular with two dorsal projections, and a concavity between them (char. 77:2), modified from Jones & Butler (2018); a double-prong suture between the dentary and surangular (char. 98:2); and dorsal transition over 20° from the dentary to the surangular (char. 99:2–3).

Another two phytosaur specimens were added to clarify their phylogenetic relationship among phytosaurs. The Iberian phytosaur NOVA-FCT-DCT 5396 was located as the non-Leptosuchomorpha sister to *Angistorhinus talainti* (Argana Basin, Morocco), supporting its classification as *Angistorhinus* cf. *talainti*. The North American specimen NMMNHS P-4256 shows similarities with Mystriosuchini phytosaurs and is recovered here within the clade *Machaeroprosopus*, consistent with previous research. Consequently, we identified the specimen as cf. *Machaeroprosopus* (Mystriosuchini).

Our phylogenetic analysis, based on landmark data, shows that there are phylogenetically informative characters in the posterior region of phytosaur mandibles. This methodology can potentially be applied to other regions of the phytosaur skeleton and could help to better resolve the phylogenetic relationships within this still enigmatic clade of Triassic archosaurs.

Acknowledgements. We are grateful to the curators of the Museu Municipal de Loulé (Portugal), the Muséum national d'Histoire naturelle of Paris (France), the Staatliches Museum für Naturkunde Stuttgart (Germany), the Institute of Paleobiology of the Polish Academy of Sciences of Warsaw (Poland), and to M. Marzola for the shared photographs. Also, we are very grateful to R. Martino, A. Guillaume and F. Rotatori for their help with the geometric morphometric, statistical and phylogenetic analyses. We are also grateful for the comments and suggestions of the reviewers and editors of the journal. This research was funded by the projects GeoBioTec–GeoBioSciences, GeoTechnologies and GeoEngineering NOVA (UIDB/04035/2020; https://doi.org/10.54499/UIDB/04035/2020) and Biogeosauria (PTDC/CTA-PAL/2217/2021) funded by the Fundação para a Ciência e a Tecnologia (Portugal). EPP was funded by SFRH/BPD/116759/2016 (Fundação para a Ciência e Tecnologia), PID2021-122612OB-I00 (Ministerio de Ciencia e Innovación, Government of Spain) and by a María Zambrano postdoctoral contract (Ministerio de Universidades of the Government of Spain through the Next Generation EU funds of the European Union). VLR was funded by the PhD Fellowship 2021.06877.BD of the Fundação para a Ciência e a Tecnologia (Portugal). Wiley and FCT/b-on have an agreement to cover the cost of your open access publishing. Please note: FCT/b-on strongly encourages you to apply a CC BY license to your article as this will amplify the article visibility and knowledge advancement, while retaining full credit of your authorship.

Author contributions. **Conceptualization** V. López-Rojas (VLR), E. Puértolas-Pascual (EPP), M. Moreno-Azanza (MMA); **Data Curation** VLR; **Formal Analysis – Morphometrics** VLR; **Formal Analysis – Phylogenetics** VLR, MMA; **Methodology**, VLR, EPP, MMA; **Project Administration**, EPP, MMA; **Comparative discussion** VLR, EPP, MMA; **Supervision**, EPP, MMA; **Funding acquisition**, MMA; **Writing – Original Draft Preparation**, VLR; **Writing – Review & Editing**, MMA, EPP, VLR.

Editor. Philip Mannion

SUPPORTING INFORMATION

Additional Supporting Information can be found online (https://doi.org/10.1002/spp2.70045):

Appendix S1. TNT files, tps files, R Studio file with all coding for running the PCAs and images of all mandibles used for landmarking, isolated and oriented in line with the tps files.

REFERENCES

Allemand, R., López-Aguirre, C., Abdul-Sater, J., Khalid, W., Lang, M. M., Macrì, S., Di-Poï, N., Daghfous, G. and Silcox, M. T. 2023. A landmarking protocol for geometric morphometric analysis of squamate endocasts. *The Anatomical Record*, **306**, 2425–2442.

Anderson, H. T. 1938. The jaw musculature of the phytosaur *Machaeroprosopus*. *Journal of Morphology*, **59**, 549–587.

Baken, E. K. 2023. gmShiny: Shiny app interface for geomorph. https://github.com/geomorphR/gmShiny

Baken, E. K., Collyer, M. L., Kaliontzopoulou, A. and Adams, D. C. 2021. geomorph v4.0 and gmShiny: enhanced analytics and a new graphical interface for a comprehensive morphometric experience. *Methods in Ecology and Evolution*, **12**, 2355–2363.

Ballew, K. L. 1989. A phylogenetic analysis of Phytosauria from the Late Triassic of the western United States. 309–339. *In* Lucas, S. G. and Hunt, A. P. (eds) *Dawn of the age of dinosaurs in the American Southwest*. New Mexico Museum of Natural History & Science.

Berrocal-Casero, M., Audije-Gil, J., Castanhinha, R. A., Pérez-Valera, J. A., Dos Santos, V. F. and Segura, M. 2018. New discoveries of vertebrate remains from the Triassic of Riba de Santiuste, Guadalajara (Spain). *Proceedings of the Geologists' Association*, **129**, 526–541.

Bona, P., Fernandez Blanco, M. V., Ezcurra, M. D., Von Baczko, M. B., Desojo, J. B. and Pol, D. 2022. On the homology of crocodylian post-dentary bones and their macroevolution throughout Pseudosuchia. *The Anatomical Record*, **305**, 2980–3001.

Bookstein, F. L. 1991. *Morphometric tools for landmark data*. Cambridge University Press, 435 pp.

Broom, R. 1913. Note on *Mesosuchus browni*, Watson, and on a new South African Triassic pseudosuchian (*Euparkeria capensis*). *Records of the Albany Museum*, **2**, 394–396.

Brusatte, S. L., Butler, R. J., Mateus, O. and Steyer, J. S. 2015. A new species of *Metoposaurus* from the Late Triassic of Portugal and comments on the systematics and biogeography of metoposaurid temnospondyls. *Journal of Vertebrate Paleontology*, **35**, e912988.

Butler, R. J., Rauhut, O. W. M., Stocker, M. R. and Bronowicz, R. 2014. Redescription of the phytosaurs *Paleorhinus* ('*Francosuchus*') *angustifrons* and *Ebrachosuchus neukami* from Germany, with implications for Late Triassic biochronology. *Zoological Journal of the Linnean Society*, **170**, 155–208.

Butler, R. J., Jones, A. S., Buffetaut, E., Mandl, G. W., Scheyer, T. M. and Schultz, O. 2019. Description and phylogenetic placement of a new marine species of phytosaur (Archosauriformes: Phytosauria) from the Late Triassic of Austria. *Zoological Journal of the Linnean Society*, **187**, 198–228.

Camargo, A. 2022. PCAtest: testing the statistical significance of principal component analysis in R. *PeerJ*, **10**, e12967.

Camargo, A. 2024. PCAtest. https://github.com/arleyc/PCAtest

Camp, C. L. 1930. A study of phytosaurs with description of new material from the Western North America. *Memoirs of the University of California*, **10**, 1–174.

Case, E. C. 1922. New reptiles and stegocephalians from the Upper Triassic of Western Texas. *Carnegie Institution of Washington*, **321**, 7–84.

Case, E. C. 1927. A complete phytosaur pelvis from the Triassic beds of Western Texas. *Contributions from the Museum of Geology University of Michigan*, **2**, 227–229.

Case, E. C. 1932. A perfectly preserved segment of the armor of a phytosaur, with associated vertebrae. *Contributions from the Museum of Paleontology*, **4**, 57–90.

Catalano, S. A., Goloboff, P. A. and Giannini, N. P. 2010. Phylogenetic morphometrics (I): the use of landmark data in a phylogenetic framework. *Cladistics*, **26**, 539–549.

Changbunjong, T., Chaiphongpachara, T. and Weluwanarak, T. 2023. Species discrimination of *Stomoxys* flies *S. bengalensis, S. calcitrans*, and *S. sitiens* (Diptera: Muscidae) using wing geometric morphometrics. *Animals*, **13**, 647.

Chatterjee, S. 1978. A primitive parasuchid (phytosaur) reptile from the Upper Triassic Maleri Formation of India. *Palaeontology*, **21**, 83–127.

Cope, E. D. 1881. *Belodon* in New Mexico. *American Naturalist*, **15**, 922–923.

Datta, D. and Ray, S. 2023. A giant phytosaur (Diapsida, Archosauria) from the Upper Triassic of India with new insights on phytosaur migration, endemism and extinction. *Papers in Palaeontology*, **9**, e1476.

Datta, D., Sharma, K. and Ray, S. 2021. Cranial evolution of the Late Triassic phytosaurs (Diapsida, Archosauria): preliminary observations from landmark-based morphometric analysis. *Historical Biology*, **33**, 2683–2705.

De Simão-Oliveira, D., Dos Santos, T., Pinheiro, F. L. and Pretto, F. A. 2024. Assessing the adductor musculature and jaw mechanics of *Proterochampsa nodosa* (Archosauriformes: Proterochampsidae) through finite element analysis. *The Anatomical Record*, **307**, 1300–1314.

Dutuit, J. M. 1977a. *Paleorhinus magnoculus*, Phytosaure du Trias supérieur de l'Atlas marocain. [*Paleorhinus magnoculus*, Phytosaurus from the Upper Triassic of the Moroccan Atlas]. *Géologie Méditerranéenne*, **4**, 255–267.

Dutuit, J. M. 1977b. Description du crene de *Angistorhinus talainti* n. sp. un nouveau Phytosaure du Trias atlasigue marocain. [Description of the skull of *Angistorhinus talainti* n. sp. a new Phytosaurus from the Moroccan Atlas Triassic]. *Bulletin du Muséum National d'Histoire Naturelle, Sciences de la Terre*, **66**, 297–337.

Dzik, J. 2001. A new *Paleorhinus* fauna in the early Late Triassic of Poland. *Journal of Vertebrate Paleontology*, **21**, 625–627.

Dzik, J. and Sulej, T. 2007. A review of the early Late Triassic Krasiejów biota from Silesia, Poland. *Palaeontologia Polonia*, **64**, 3–27.

Ezcurra, M. D. 2016. The phylogenetic relationships of basal archosauromorphs, with an emphasis on the systematics of proterosuchian archosauriforms. *PeerJ*, **4**, e1778.

Ezcurra, M. D., Fortuny, J., Mujal, E. and Bolet, A. 2017. First direct archosauromorph remains from the early-middle Triassic transition of the Iberian Peninsula. *Palaeontologia Electronica*, **20** (3), 62A.

Fara, E. and Hungerbühler, A. 2000. *Paleorhinus magnoculus* from the Upper Triassic of Morocco: a juvenile primitive phytosaur (Archosauria). *Comptes Rendus de l'Académie des Sciences – Series IIA – Earth and Planetary Science*, **331**, 831–836.

Fraas, E. 1896. Die Schwäbischen Trias–Saurier nach dem Material der Kgl. Naturalien Sammlung in Stuttgart zusammengestelt. [The Swabian Triassic dinosaurs according to the material of the Royal Natural history collection compiled in Stuttgart.]. *Mitteilungen aus dem Koniglichen Naturalienkabinett zu Stuttgart*, **5**, 1–18.

Goldsmith, E. R., Barta, D. E., Kligman, B. T., Nesbitt, S. J., Marsh, A. D., Parker, W. G. and Stocker, M. R. 2024. Osteohistological signal from the smallest known phytosaur femur reveals slow growth and new insights into the evolution of growth in Archosauria. *Journal of Anatomy*, **247**, 556–575.

Goloboff, P. A. and Catalano, S. A. 2011. Phylogenetic morphometrics (II): algorithms for landmark optimization. *Cladistics*, **27**, 42–51.

Goloboff, P. A. and Morales, M. 2023. TNT version 1.6, with a graphical interface for MacOs and Linux, including new routines in parallel. *Cladistics*, **39**, 144–153.

Gozzi, E. and Renesto, S. 2003. A complete specimen of *Mystriosuchus* (Reptilia, Phytosauria) from the Norian (Late Triassic) of Lombardy (Northern Italy). *Rivista Italiana di Paleontologia e Stratigrafia*, **109**, 475–491.

Griffin, C. T., Stefanic, C. M., Parker, W. G., Hungerbühler, A. and Stocker, M. R. 2017. Sacral anatomy of the phytosaur *Smilosuchus adamanensis*, with implications for pelvic girdle evolution among Archosauriformes. *Journal of Anatomy*, **231**, 886–905.

Heckert, A. B., Lucas, S. G., Hunt, A. P. and Harris, J. D. 2001. A giant phytosaur (Reptilia: Archosauria) skull from the Redonda Formation (Upper Triassic: Apachean) of east-central New Mexico. New Mexico Geological Society Guidebook, 52nd Field Conference, Geology of Llano Estacado, 169–176.

Heckert, A. B., Jenkins, H. and Hunt, A. P. 2013. Mandibles of juvenile phytosaurs (Archosauria: Crurotarsi) from the Upper Triassic Chinle Group of Texas and New Mexico, USA. *New Mexico Museum of Natural History & Science Bulletin*, **61**, 228–235.

Heckert, A. B., Viner, T. C. and Carrano, M. T. 2021. A large, pathological skeleton of *Smilosuchus gregorii* (Archosauriformes: Phytosauria) from the Upper Triassic of Arizona, U.S.A., with discussion of the paleobiological implications of

paleopathology in fossil archosauromorphs. *Palaeontologia Electronica*, **24** (2), 21A.

Holliday, C. M. 2019. New insights into dinosaur jaw muscle anatomy. *The Anatomical Record*, **292**, 1246–1265.

Holliday, C. M., Sellers, K. C., Lessner, E. J., Middleton, K. M., Cranor, C., Verhulst, C. D., Lautenschlager, S., Bader, K., Brown, M. A. and Colbert, M. W. 2022. New frontiers in imaging, anatomy, and mechanics of crocodylian jaw muscles. *The Anatomical Record*, **305**, 3016–3030.

Holloway, W. L. 2018. Comparative cranial ecomorphology and functional morphology of semiaquatic faunivorous crurotarsans. PhD thesis. Faculty of the College of Arts and Sciences, Ohio University, USA, 270 pp. http://rave.ohiolink.edu/etdc/view?acc_num=ohiou1542230980102513

Holvast, E. J., Celik, M. A., Phillips, M. J. and Wilson, L. A. B. 2024. Do morphometric data improve phylogenetic reconstruction? A systematic review and assessment. *BMC Ecology and Evolution*, **24**, 127.

Hungerbühler, A. 1998. Cranial anatomy and diversity of the Norian phytosaurs of Southwestern Germany. PhD thesis. University of Bristol, UK, 360 pp. https://hdl.handle.net/1983/616827dd-9e4c-42e5-aec2-bf85cf54c52d

Hungerbühler, A. 2000. Heterodonty in the European phytosaur *Nicrosaurus kapffi* and its implications for the taxonomic utility and functional morphology of phytosaur dentitions. *Journal of Vertebrate Paleontology*, **20**, 31–48.

Hungerbühler, A. 2002. The Late Triassic phytosaur *Mystriosuchus westphali*, with a revision of the genus. *Palaeontology*, **45**, 377–418.

Hungerbühler, A., Mueller, B., Chatterjee, S. and Cunningham, D. P. 2013. Cranial anatomy of the Late Triassic phytosaur *Machaeroprosopus*, with the description of a new species from West Texas. *Earth and Environmental Science Transactions of the Royal Society of Edinburgh*, **103**, 269–312.

Hunt, A. P. 1994. Vertebrate paleontology and biostratigraphy of the Bull Canyon Formation (Chinle Group, Upper Triassic), East-Central New Mexico with revisions of the families Metoposauridae (Amphibia: Temnospondyli) and Parasuchidae (Reptilia: Archosauria). PhD thesis. The University of New Mexico, Albuquerque, 404 pp.

Hunt, A. P. and Lucas, S. G. 1993. Stratigraphy and vertebrate paleontology of the Chinle Group (Upper Triassic), Chama Basin, North-Central New Mexico. *Vertebrate Paleontology in New Mexico*, **2**, 61–69.

Hunt, A. P., Lucas, S. G. and Heckert, A. B. 2002. A Revueltian (Norian) phytosaur from the Sonsela Member of the Petrified Forest Formation (Chinle Group: Upper Triassic), Petrified Forest National Park, Arizona. *New Mexico Museum of Natural History & Science Bulletin*, **21**, 165–169.

Hunt, A. P., Lucas, S. G. and Spielmann, J. A. 2006. Sexual dimorphism in a large brachyrostral phytosaur (Archosauria: Crurotarsi) from the Late Triassic of Western North America. *New Mexico Museum of Natural History & Science Bulletin*, **37**, 563–567.

Jansky, K., Schubert, B. W. and Wallace, S. C. 2016. Geometric morphometrics of dentaries in *Myotis*: species identification and its implications for conservation and the fossil record. *Northeastern Naturalist*, **23**, 184–194.

Jones, A. S. and Butler, R. J. 2018. A new phylogenetic analysis of Phytosauria (Archosauria: Pseudosuchia) with the application of continuous and geometric morphometric character coding. *PeerJ*, **6**, e5901.

Kammerer, C. F., Butler, R. J., Bandyopadhyay, S. and Stocker, M. R. 2016. Relationships of the Indian phytosaur *Parasuchus hislopi* Lydekker, 1885. *Papers in Palaeontology*, **2**, 1–23.

Kimmig, J. 2013. Possible secondarily terrestrial lifestyle in the European phytosaur *Nicrosaurus kapffi* (Late Triassic, Norian): a preliminary study. *New Mexico Museum of Natural History & Science Bulletin*, **61**, 306–312.

Kobayashi, Y., Takasaki, R., Fiorillo, A. R., Chinzorig, T. and Hikida, Y. 2022. New therizinosaurid dinosaur from the marine Osoushinai Formation (Upper Cretaceous, Japan) provides insight for function and evolution of therizinosaur claws. *Scientific Reports*, **12**, 7207.

Kuhn, O. 1936. Weitere Parasuchier und Labyrinthodonten aus dem Blasensandstein des mittleren Keuper von Ebrach [Further Parasuchia and Labyrinthodontia from the middle Keuper bubble sandstone from Ebrach]. *Palaeontographica Abteilung A*, **83**, 61–98.

Langston, W. Jr 1949. A new species of *Paleorhinus* from the Triassic of Texas. *American Journal of Science*, **247**, 324–341.

Lemanis, R., Jones, A. S., Butler, R. J., Anderson, P. S. L. and Rayfield, E. J. 2019. Comparative biomechanical analysis demonstrates functional convergence between slender-snouted crocodilians and phytosaurs. *PeerJ Preprints*, **7**, e27476v1.

LePore, C. N. and McLain, M. A. 2024. Variation in the sacrum of phytosaurs: new evidence from a partial skeleton of *Machaeroprosopus mccauleyi*. *Journal of Anatomy*, **244**, 959–976.

Li, C., Wu, X. C., Zhao, L. J., Sato, T. and Wang, L. T. 2012. A new archosaur (Diapsida, Archosauriformes) from the marine Triassic of China. *Journal of Vertebrate Paleontology*, **32**, 1064–1081.

Long, A. R. and Murry, P. A. 1995. *Late Triassic (Carnian and Norian) tetrapods from the southwestern United States*. New Mexico Museum of Natural History & Science, Bulletin 4, 254 pp.

López-Rojas, V., Clemmensen, L. B., Milàn, J., Wings, O., Klein, N. and Mateus, O. 2022. A new phytosaur species (Archosauriformes) from the Upper Triassic of Jameson Land, central East Greenland. *Journal of Vertebrate Paleontology*, **42**, e2181086.

Lydekker, R. 1885. The reptilia & amphibia of the Maleri & Denwa groups. *Palaeontologia Indica, Series 4*, **1**, 1–38.

Maiorino, L., Farke, A. A., Kotsakis, T. and Piras, P. 2013. Is *Torosaurus Triceratops*? Geometric morphometric evidence of late Maastrichtian ceratopsid dinosaurs. *PLoS One*, **8**, e81608.

Martinez Arbizu, P. 2020. pairwiseAdonis: Pairwise multilevel comparison using adonis. R package version 0.4. https://github.com/pmartinezarbizu/pairwiseAdonis

Mateus, O., Butler, R. J., Brusatte, S. L., Whiteside, J. H. and Steyer, J. S. 2014. The first phytosaur (Diapsida, Archosauriformes) from the Late Triassic of the Iberian Peninsula. *Journal of Vertebrate Paleontology*, **34**, 970–975.

McGuire, J. L. 2011. Identifying California *Microtus* species using geometric morphometrics documents quaternary geographic range contractions. *Journal of Mammalogy*, **92**, 1383–1394.

Mehl, M. G. 1928. The Phytosauria of the Wyoming Triassic. *Journal of the Denison University Laboratories, Denison University*, **23**, 141–172.

Meyer, H. von 1860. Briefliche Mittheilung an Prof. Bronn. *Neues Jahrbuch fur Mineralogie, Geognosie, Geologie und Petrefakten-Kunde*, **1860**, 556–560.

Meyer, H. von 1863. Der Schädel des *Belodon* aus dem Stubensandstein des oberen Keupers. [The skull of *Belodon* from the Stubensandstein of the upper Keuper.]. *Palaeontographica*, **10**, 227–246.

Nesbitt, S. J. 2011. The early evolution of archosaurs: relationships and the origin of major clades. *Bulletin of the American Museum of Natural History*, **352**, 1–292.

Nomade, S., Knight, K. B., Beutel, E., Renne, P. R., Verati, C., Feraud, G., Marzoli, A., Youbi, N. and Bertrand, H. 2007. Chronology of the Central Atlantic Magmatic Province: implications for the Central Atlantic rifting processes and the Triassic–Jurassic biotic crisis. *Palaeogeography, Palaeoclimatology, Palaeoecology*, **244**, 326–344.

Pandolfi, L., Martino, R., Rook, L. and Piras, P. 2020. Investigating ecological and phylogenetic constraints in Hippopotamidae skull shape. *Rivista Italiana di Paleontologia e Stratigrafia*, **126**, 37–49.

Parker, W. G. and Irmis, R. B. 2006. A new species of the Late Triassic phytosaur *Pseudopalatus* (Archosauria: Pseudosuchia) from Petrified Forest National Park, Arizona. *Museum of Northern Arizona Bulletin*, **62**, 126–143.

Parker, W. G., Hungerbühler, A. and Martz, J. W. 2013. The taxonomic status of the phytosaurs (Archosauriformes) *Machaeroprosopus* and *Pseudopalatus* from the Late Triassic of the western United States. *Earth and Environmental Science Transactions of the Royal Society of Edinburgh*, **103**, 265–268.

Pereira-Pedro, A. S., Bruner, E., Gunz, P. and Neubauer, S. 2020. A morphometric comparison of the parietal lobe in modern humans and Neanderthals. *Journal of Human Evolution*, **142**, 102770.

Prieto-Márquez, A., Garcia-Porta, J., Joshi, S. H., Norell, M. A. and Makovicky, P. J. 2020. Modularity and heterochrony in the evolution of the ceratopsian dinosaur frill. *Ecology and Evolution*, **10**, 6288–6309.

Rinehart, L. F., Lucas, S. G., Heckert, A. B., Spielmann, J. A. and Celeskey, M. D. 2009. The Paleobiology of *Coelophysis bauri* (Cope) from the Upper Triassic (Apachean) Whitaker quarry, New Mexico, with detailed analysis of a single quarry block. *New Mexico Museum of Natural History & Science Bulletin*, **45**, 1–260.

Rohlf, F. J. 2017. tpsDig, digitize landmarks and outlines, version 2.31. Department of Ecology and Evolution, State University of New York at Stony Brook.

Rohlf, F. J. 2022. tpsUtil, file utility program. version 1.842. Department of Ecology and Evolution, State University of New York at Stony Brook.

RStudio Team. 2020. RStudio: Integrated Development for R. RStudio, PBC, Boston, MA.

Schlager, S. 2014. Morpho: Calculations and visualisations related to Geometric Morphometrics. R-package version 2.0.3-1. https://cran.r-project.org/package=Morpho

Sellers, K. C., Nieto, M. N., Degrange, F. J., Pol, D., Clark, J. M., Middleton, K. M. and Holliday, C. M. 2022. The effects of skull flattening on suchian jaw muscle evolution. *The Anatomical Record*, **305**, 2791–2822.

Stocker, M. R. 2010. A new taxon of phytosaur (Archosauria: Pseudosuchia) from the Late Triassic (Norian) Sonsela Member (Chinle Formation) in Arizona, and a critical reevaluation of *Leptosuchus* Case, 1922. *Palaeontology*, **53**, 997–1022.

Stocker, M. R. 2012. A new phytosaur (Archosauriformes, Phytosauria) from the Lots Wife beds (Sonsela Member) within the Chinle Formation (Upper Triassic) of Petrified Forest National Park, Arizona. *Journal of Vertebrate Paleontology*, **32**, 573–586.

Stocker, M. R. 2013. A new taxonomic arrangement for *Paleorhinus scurriensis*. *Earth and Environmental Science Transactions of the Royal Society of Edinburgh*, **103**, 251–263.

Stocker, M. R. and Butler, R. J. 2013. Phytosauria. *Geological Society Special Publication*, **379**, 91–117.

Stocker, M. R., Zhao, L. J., Nesbitt, S. J., Wu, X. C. and Li, C. 2017. A short-snouted, Middle Triassic phytosaur and its implications for the morphological evolution and biogeography of Phytosauria. *Scientific Reports*, **7**, 46028.

Terrinha, P., Ribeiro, C., Kullberg, J. C., Lopes, C., Rocha, R. and Ribeiro, A. 2002. Compressive episodes and faunal isolation during rifting, Southwest Iberia. *The Journal of Geology*, **110**, 101–113.

Uyeda, J. C., Caetano, D. S. and Pennell, M. W. 2015. Comparative analysis of principal components can be misleading. *Systematic Biology*, **64**, 677–689.

Verati, C., Rapaille, C., Feraud, G., Marzoli, A., Bertrand, H. and Youbi, N. 2007. 40Ar/39Ar ages and duration of the Central Atlantic Magmatic Province volcanism in Morocco and Portugal and its relation to the Triassic–Jurassic boundary. *Palaeogeography, Palaeoclimatology, Palaeoecology*, **244**, 308–325.

Vilas-Boas, M., Pereira, Z., Cirilli, S. and Fernandes, P. 2024. New insights on the Upper Triassic Silves Group in Algarve Basin, Portugal: palynological, paleophytogeography and paleoclimatology advances. *Geobios*, **86**, 49–64.

Yun, C.-G. 2024. *Spinosaurus* as phytosaur mimics: a case of convergent evolution between two extinct archosauriform clades. *Acta Palaeontologica Romaniae*, **20**, 17–29.

Zeigler, K. E., Lucas, S. G. and Heckert, A. B. 2002. The Late Triassic Canjilon quarry (Upper Chinle Group, New Mexico) phytosaur skulls: evidence of sexual dimorphism in phytosaurs. *New Mexico Museum of Natural History & Science Bulletin*, **21**, 179–188.

Zeigler, K. E., Heckert, A. B. and Lucas, S. G. 2003. Phytosaur (Archosauria: Parasuchidae) cranial and mandibular material from the Upper Triassic Snyder Quarry (Petrified Forest Formation, Chinle Group). *New Mexico Museum of Natural History & Science Bulletin*, **24**, 81–88.